Article

Three-Dimensional Printable Conductive Semi-Interpenetrating Polymer Network Hydrogel for Neural Tissue Applications

Chiara Rinoldi, Massimiliano Lanzi, Roberto Fiorelli, Paweł Nakielski, Krzysztof Zembrzycki, Tomasz Kowalewski, Olga Urbanek, Valentina Grippo, Katarzyna Jezierska-Woźniak, Wojciech Maksymowicz, Andrea Camposeo, Renata Bilewicz, Dario Pisignano, Nader Sanai, and Filippo Pierini*
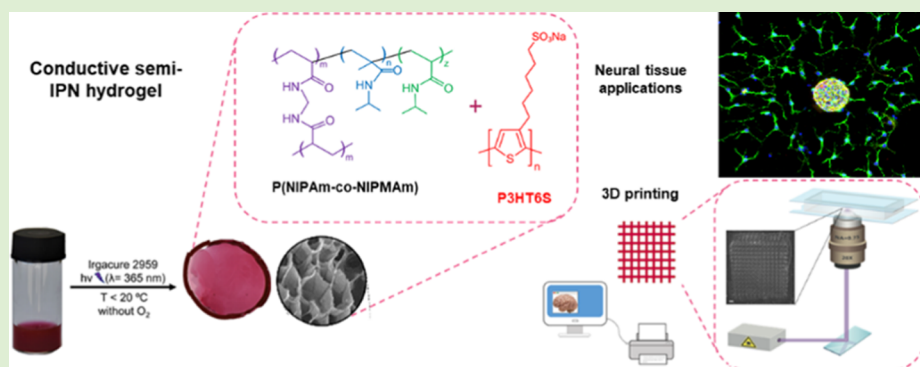
ACCESS | Metrics & More | Article Recommendations | SI Supporting Information

ABSTRACT: Intrinsically conducting polymers (ICPs) are widely used to fabricate biomaterials; their application in neural tissue engineering, however, is severely limited because of their hydrophobicity and insufficient mechanical properties. For these reasons, soft conductive polymer hydrogels (CPHs) are recently developed, resulting in a water-based system with tissue-like mechanical, biological, and electrical properties. The strategy of incorporating ICPs as a conductive component into CPHs is recently explored by synthesizing the hydrogel around ICP chains, thus forming a semi-interpenetrating polymer network (semi-IPN). In this work, a novel conductive semi-IPN hydrogel is designed and synthesized. The hybrid hydrogel is based on a poly(*N*-isopropylacrylamide-*co*-*N*-isopropylmethacrylamide) hydrogel where polythiophene is introduced as an ICP to provide the system with good electrical properties. The fabrication of the hybrid hydrogel in an aqueous medium is made possible by modifying and synthesizing the monomers of polythiophene to ensure water solubility. The morphological, chemical, thermal, electrical, electrochemical, and mechanical properties of semi-IPNs were fully investigated. Additionally, the biological response of neural progenitor cells and mesenchymal stem cells in contact with the conductive semi-IPN was evaluated in terms of neural differentiation and proliferation. Lastly, the potential of the hydrogel solution as a 3D printing ink was evaluated through the 3D laser printing method. The presented results revealed that the proposed 3D printable conductive semi-IPN system is a good candidate as a scaffold for neural tissue applications.

1. INTRODUCTION

Intrinsically conducting polymers (ICPs) have been attracting much attention due to their interesting electronic, mechanical, thermal, optical, and chemical properties that make possible a broad range of applications, including organic electronics, photovoltaics, sensors, catalysis, and batteries.[1−4] More recently, a few biocompatible ICPs[5−7] were proposed for promoting the conduction of electrical signals in physiologic environments.[8,9] This application plays a pivotal role in biological processes, including neural communication and neural tissue repair.[10,11]

While ICPs have been widely used to fabricate biomaterials,[12−14] their application in neural tissue engineering is severely limited because of ICPs' insufficient mechanical properties:[15] the neural tissue is intrinsically soft (1−10 kPa for brain slices),[16] while the Young's Modulus of ICP materials is several orders of magnitude higher than that of neural tissues.[17,18] Upon implantation, the stiffer properties of ICP materials might trigger injury-response mechanisms in the brain tissue, leading to scaffold encapsulation and subsequent

isolation from living tissues.[19] Researchers' efforts to reduce the Young's Modulus of conductive biomaterials from GPa to kPa resulted in the development of a class of soft conducting materials called conductive polymer hydrogels (CPHs).[20]

To address such challenges, CPHs were designed to have the beneficial synergistic characteristics of hydrogel structures and conductive polymers, resulting in a system with outstanding adhesion, porosity, and electrical properties.[21−23] Additionally, CPHs have suitable physical and biological properties, including tissue-like mechanical features, high water content, and biocompatibility.[24] For these reasons, CPHs are considered promising biomaterials for the fabrication of next generation scaffolds for neural tissue engineering.[25−27]

CPHs have been easily synthesized by combining a hydrogel precursor with conductive nanofillers (e.g., graphene oxide,[28] carbon nanotubes,[29] and nanoparticles[30]), even though a high filler concentration is required to form an electrically conductive network. The drastic mismatch between the nanofiller stiffness and the polymer weakens the composite hydrogel mechanical properties, resulting in a brittle and physically unstable composite.[31] Furthermore, the introduction of carbonaceous nanofillers into neural biomaterials is questionable because of possible cytotoxic effects.[32,33]

Another approach is to incorporate ICPs as a conductive component into CPHs, basically via two strategies: (i) polymerization of ICP monomers within the hydrogel matrix[34] and (ii) embedding ICP chains during the hydrogel polymerization process.[35] In the first case, the final CPH has poor and inhomogeneous electrical properties and weak mechanical characteristics, while the second method leads to a relatively low hydrogel conductivity.[36]

Recently, a novel method to integrate ICPs successfully into the hydrogel matrix was developed by synthesizing the hydrogel surrounding ICP chains, thus forming a semi-interpenetrating polymer network (semi-IPN).[37,38] Compared to other CPHs, semi-IPNs exhibit a high chemical and mechanical stability with outstanding biocompatibility and electrical and electrochemical properties.[39,40] Moreover, this approach has several advantages, such as the use of already purified ICPs with an optimized regiochemical structure, the possibility to fabricate complex three-dimensional (3D) structures (e.g. using 3D printing), and its easy, low-cost preparation.[41,42] The fabrication of conductive semi-IPN, however, entails some significant difficulties related to ICP hydrophobicity and low solubility in water.[43,44] Polythiophenes (PTs) appear particularly suitable for addressing such issues because one can easily modify the repeating units by attaching ionic pendant groups to the flexible side chains and synthesize water-soluble ICPs with sufficient electronic properties.[45,46]

On the other hand, with regard to the hydrogel component, poly(N-isopropylacrylamide) (PNIPAm) hydrogel has been successfully used for biomedical applications.[47,48] Its advantages, such as its mechanical properties similar to those of living tissue, biocompatibility, high porosity, and high water content have shown that the PNIPAm hydrogel matrix is a great option for synthesizing and creating 3D structures with complex architectures made of CPHs.[49−51]

In light of this, we designed, synthesized, fabricated, and characterized a novel conductive semi-IPN hydrogel. Specifically, our hybrid hydrogel is based on a poly(N-isopropylacrylamide-co-N-isopropylmethacrylamide) (P(NIPAm-co-NIPMAm)) hydrogel, to which sodium poly[6-(3-thienyl)-hexanesulfonate] (P3HT6S) was added as an ICP component

to provide the system with good electrical properties. The morphological, chemical, electrical, and mechanical properties of the semi-IPN were fully characterized. Lastly, the biological responses of neural progenitor cells (NPCs) and human Wharton's jelly-derived mesenchymal stem cells (hWJ-MSCs) in contact with the conductive semi-IPN were investigated. The developed hybrid hydrogel was demonstrated to be exploitable as a UV-curable ink for light exposure-based printing, thus opening exciting perspectives for the fabrication of 3D biomaterials with complex geometries and tailored physical properties.

2. MATERIALS AND METHODS

2.1. Materials. All materials were purchased from Sigma-Aldrich unless specified. Disodium phosphate and sodium chloride (NaCl) were obtained from POCh (Polish Chemicals Co., Gliwice, Poland). The double-distilled water used throughout the study had a resistance greater than 18 MΩ·cm (Milli Q Water, 18.2 MΩ cm^{-1}, Millipore, Bedford, MA, USA). Before use, monomers and the cross-linking agent were purified by repeated recrystallization from hexane and methanol, respectively, and dried in a vacuum. Only analytical grade chemicals were used.

2.2. Synthesis of Sodium Poly[6-(3-thienyl)-hexanesulfonate]. P3HT6S (HT dyads: 95%, Mn: 29200 g/mol; PDI: 1.28; DPn: 118) was prepared following the procedure described by Lanzi et al.[52] Briefly, 0.438 g (1.79 mmol) of regioregular poly[3-(6-bromohexyl)thiophene] was added to 40 mL of anhydrous tetrahydrofuran (THF) with 0.250 g (1.98 mmol) of sodium sulfite (Na$_2$SO$_3$). The mixture was refluxed for 72 h under stirring. After solvent evaporation at reduced pressure, the obtained polymer was poured into a glass Gooch filter crucible (G3) and washed several times with a solution of hydrochloric acid in methanol (10% v/v), resulting in 0.331 g (1.34 mmol) of P3HT6S (75% yield).

2.3. Preparation of P(NIPAm-co-NIPMAm)/P3HT6S Hydrogels. P(NIPAm-co-NIPMAm)/P3HT6S hydrogels were prepared by radical polymerization, covalently cross-linking NIPAm and NIPMAm monomers in the presence of UV light. Briefly, 2.04 mg of P3HT6S were added to 1.0 mL of a tetrahydrofuran/water (5:95) mixture. The solution was placed in a sealed vial and positioned in a silicon oil bath at 50 °C. P3HT6S was subjected to constant stirring until complete dissolution. The solution was cooled down to room temperature, where the reddish solution remained clear and in liquid state. Then, N-isopropylacrylamide (NIPAm, monomer, 46.25 mg, 0.409 mmol, 92.5 wt % of the final polymer composition), N-isopropylmethacrylamide (NIPMAm, monomer, 1.25 mg, 0.010 mmol, 2.5 wt % of the final polymer composition), N,N′-methylenebis(acrylamide) (BIS, cross-linking agent, 2.5 mg, 0.016 mmol, 5.0 wt % of the final polymer composition), and 2-hydroxy-4′-(2-hydroxyethoxy)-2-methylpropiophenone (Irgacure 2959, photoinitiator, 10 mg, 0.044 mmol) were dissolved in the previously prepared P3HT6S solution (1.0 mL). The precursor hydrogel solution was made of 5 wt % polymer components (including monomers and the initiator cross-linking agent) in distilled water. After being stirred for 24 h, the precursor solution was purged with argon gas for 30 min to remove oxygen and tetrahydrofuran traces. The polymer mix was photo-cross-linked, exposing the solution to UV irradiation at a distance of 20 cm from the light source for 1 min (λmax = 365 nm, light intensity of 225 mW/cm^2, Dymax 5000-EC Series UV curing flood lamp). During the polymerization process, the temperature was kept below 20 °C by using an iced water bath to control the hydrogel synthesis and avoid network heterogeneity at the molecular level. Lastly, different hydrogels were prepared by varying the concentration of P3HT6S to fabricate a reference material without including the polythiophene derivative and to optimize CPH concentration. For this purpose, an optimized amount of P3HT6S was added to the P(NIPAm-co-NIPMAm) hydrogel precursor solution. Sample codes and detailed recipes used in this work are shown in Table S1.

2.4. Morphological Evaluation of P(NIPAm-co-NIPMAm)/P3HT6S Hydrogel. The hydrogel porous structure was examined by

means of field emission scanning electron microscopy (FE-SEM, FEI Nova NanoSEM 450) operating at 10 kV. Fully swollen hydrogels were frozen in liquid nitrogen and then freeze-dried. Subsequently, samples were longitudinally cut to expose their cross section. The synthesized structures were then coated with a thin layer of gold (5 nm thick) and imaged using FE-SEM. Ten FE-SEM images per sample were collected to quantitatively investigate the morphological features of hydrogel structures by using National Institutes of Health ImageJ software. The pore aspect ratio and wall thickness were quantified using the line tool, while the void area of FE-SEM micrographs was calculated to evaluate the porosity of the material.

2.5. Physical–Chemical Characterization of P(NIPAm-*co*-NIPMAm)/P3HT6S Hydrogels. *2.5.1. Photoinitiator Release.* The cross-linked P(NIPAm-co-NIPMAm) and P(NIPAm-co-NIPMAm)/P3HT6S hydrogels were immersed in water to remove any unreacted material. At each time point, the water storage medium was subjected to UV−vis spectroscopy for the detection of photoinitiator and monomer residues. The water was changed, and the UV−vis analysis was repeated until no peak corresponding to the impurities was detected.

2.5.2. Nuclear Magnetic Resonance. [1]H and ^{13}C nuclear magnetic resonances (NMRs) of the P3HT6S polymer, as well as of the soluble fraction of P(NIPAm-*co*-NIPMAm) and P(NIPAm-*co*-NIPMAm)/P3HT6S hydrogels in D_2O, were recorded at room temperature on a Varian Mercury 400 spectrometer at 400 MHz. Chemical shifts were expressed in δ (ppm) and referred to TMS.

2.5.3. X-ray Diffraction. Wide-angle X-ray scattering measurements were obtained using a Bruker D8 Discover diffractometer in reflection mode (CuKa radiation, l [1/4] 1.5418 Å). Two theta scans were assessed by placing and fixing P(NIPAm-*co*-NIPMAm) and P(NIPAm-*co*-NIPMAm)/P3HT6S hydrogels in the center of a goniometric circle, while source and detector were moving symmetrically. Scans were conducted in the 3−34° angular range and analyzed by Origin software. P(NIPAm-*co*-NIPMAm) and P(NIPAm-*co*-NIPMAm)/P3HT6S hydrogels were tested in both hydrated and dry states.

2.5.4. Gel Permeation Chromatography. The molecular weights of the P3HT6S polymer and soluble fraction of P(NIPAm-*co*-NIPMAm) and P(NIPAm-*co*-NIPMAm)/P3HT6S hydrogels were determined by gel permeation chromatography (GPC). THF solutions were applied to a Linear Instruments UVIS-200 apparatus operating at 254 nm and equipped with a Phenomenex mixed bed column 5 μ MXL type. The GPC calibration curve was recorded using monodisperse polystyrene standards.

Differential scanning calorimetry (DSC) was used to determine the characteristic temperatures of the P(NIPAm-*co*-NIPMAm) and P(NIPAm-*co*-NIPMAm)/P3HT6S hydrogels. DSC measurements were obtained using a Perkin Elmer PYRIS-1 instrument. The analysis of hydrated samples was performed in a heating mode starting from 20 to 50 °C following a rate of 2 °/min, with an isothermal stop for 1 min. DSC analysis of freeze-dried samples was performed in the 0−250 °C range with a rate of 10 °/min.

Thermogravimetric analysis (TGA) was performed using a Q5000 (TA Instruments) instrument under a nitrogen atmosphere. Thermogravimetric measurements were carried out in the temperature range of 20−700 °C to analyze the P3HT6S polymer as well as P(NIPAm-*co*-NIPMAm) and P(NIPAm-*co*-NIPMAm)/P3HT6S hydrogels having a mass of about 2.7–3.7 mg. TGA data were analyzed using TA Universal Analysis software. All measurements were performed at a constant heating rate of 20 °C/min.

2.5.5. Swelling Profile. A swelling test was performed to evaluate the water absorption capacity of the hydrogels. Dry samples of P(NIPAm-*co*-NIPMAm) and P(NIPAm-*co*-NIPMAm)/P3HT6S hydrogels were placed and incubated in an aqueous medium for up to 15 h at room temperature. At each time point, samples were gently dried with a KIMTECH wipe and weighed with a high-precision scale.

The swelling ratio was calculated using the following formula:

$$\text{swelling ratio } \% = \frac{Wf - Wd}{Wd} \times 100 \qquad (1)$$

where *Wf* is the final weight, while *Wd* is the initial dry weight.

2.5.6. Nanomechanical Property Assessment. Atomic force microscope (AFM) nanoindentation analysis was performed to quantify the Young's Modulus of the fully hydrated P(NIPAm-*co*-NIPMAm) and P(NIPAm-*co*-NIPMAm)/P3HT6S hydrogels. Mechanical properties were measured using AFM (Ntegra, NT-MDT) in a closed liquid cell to avoid hydrogel dehydrogenation and sample contamination. A pre-calibrated CSG01 (NT-MDT) cantilever with a nominal tip radius of 6 nm and a spring constant of 0.039 N/m was used. Selected hydrogels were tested by performing at least 50 nanoindentations from 10 different surface areas per sample. The Young's moduli were calculated by fitting the Hertz model to the acquired loading curve data.

2.5.7. Electrical Impedance Test. The electrical properties of the synthesized hydrogel samples were evaluated by means of impedance measurements using a Keysight E4990A impedance analyzer (Keysight Technologies). P(NIPAm-*co*-NIPMAm) and P(NIPAm-*co*-NIPMAm)/P3HT6S hydrogels were individually located between two conductive glass slides (indium tin oxide coated, ITO, Sigma, 15−25 Ω/sq) connected with the impendence analyzer. Impedance values were detected between 1 Hz and 10 kHz range of frequency. Measurements were repeated on 10 different samples for each hydrogel condition.

2.6. Electrochemical Measurements. *2.6.1. Samples and Setup Preparation.* P(NIPAm-*co*-NIPMAm) and P(NIPAm-*co*-NIPMAm)/P3HT6S hydrogels were directly polymerized on glassy carbon electrodes (GCEs) with the help of custom-designed Teflon caps (Figure S1a). A three-electrode arrangement was used. It consisted of an Ag/AgCl (KCl sat.) reference electrode (potential of 0.197 V vs NHE[53,54]), a platinum sheet as a counter electrode, and a 3 mm-diameter GCE from BASi (West Lafayette, USA). The GCE was mechanically polished with 1.0, 0.3, and 0.05 μm alumina powder (Struers, Krakow, Poland) using a polishing cloth (Buehler, Illinois, USA). After polishing, it was rinsed with MilliQ water and sonicated in pure ethanol for 1 min. Prior to modification, the electrodes were kept in ice, while the hydrogel solution was carefully deoxygenated with argon. P(NIPAm-*co*-NIPMAm) and P(NIPAm-*co*-NIPMAm)/P3HT6S hydrogel precursors were placed on the electrode surface and polymerized under UV lamp irradiation. The polymer-covered electrodes were washed several times with MilliQ water to remove any unreacted material and/or initiator traces. The initiator removal was confirmed by following the disappearance of the initiator related band at approximately 280 nm in the UV spectrum of the water in contact with the film-covered electrodes.[55]

2.6.2. Electrochemical Tests. Cyclic voltammetry (CV) and differential pulse voltammetry (DPV) experiments were conducted using an Autolab potentiostat (Metrohm Autolab, B.V., Utrecht, The Netherlands). A 0.1 M phosphate-buffer saline solution at pH 7.4 (PBS) modified with 0.1 M NaCl was used as the electrolyte solution in all electrochemical experiments (Figure S1b). It was not possible to measure the prepared hydrogels in acetonitrile (as reported by Lanzi *et al.*[46]) due to the dehydration and degradation of the hydrogel networks in this solvent (Figure S1c). Chemical doping was performed by holding the hydrogel-modified electrodes in a 0.1 M perchloric acid ($HClO_4$) solution for 24 h. The electrodes were then washed in a PBS buffer solution. Electrochemical measurements were obtained using 5 mM potassium ferricyanide ($K_3[Fe(CN)_6]$, FCN) in PBS. Electrochemical doping was performed by exposing the hydrogel-modified electrodes to +2 V potential in a PBS solution. This value of potential was chosen because CV literature data report an oxidation peak around +1.5 V for thin P3HT6S films.[56] Thus, considering the hydrogel coating's millimetric thickness, the electrochemical doping was set at +2 V versus Ag/AgCl (KCl sat.) for 60 s; the potential scanning was applied between +2 V and −2 V (1 or 50 cycles doping). Electrodes were tested in a PBS solution containing 5 mM FCN.

All electrochemical tests were conducted at 25 °C.

2.7. Mesenchymal Stem Cell Culture. *2.7.1. Isolation and Culture of Human Wharton's Jelly-Derived Mesenchymal Stem Cells.* Human umbilical cords (n = 3) were obtained aseptically from uncomplicated full-term pregnancies delivered by a planned cesarean section. Cells were isolated using the explant isolation method, as

C

described elsewhere, with minor modifications.[57,58] This protocol was approved by the Ethics Committee of the University of Warmia and Mazury in Olsztyn and all participants gave written informed consent before their inclusion in this study. The umbilical cords were immersed in a sterile vessel containing a 0.01 M phosphate-buffered saline (PBS, pH 7.2) supplemented with 1% penicillin−streptomycin (P/S, 10000:10000; Sigma Aldrich) and then transferred to the laboratory for further cell isolation. After removing cord blood, amniotic membrane, umbilical arteries, veins, and vessels, the remaining tissue was aseptically stored in sterile PBS to wash away any contaminating blood. The cords were cut into small pieces (1−2 cm in length). The tissue pieces were transferred to 60 × 15 mm Petri dishes containing Dulbecco's Modified Eagle Medium/Nutrient Mixture F-12 (DMEM/F-12, GlutaMAX) supplemented with 1% penicillin−streptomycin (PS) and 10% fetal bovine serum (FBS, Sigma Aldrich) and incubated at 37 °C in a humidified atmosphere containing 5% CO_2. Explants were left undisturbed for 14 days to enable cell migration. Afterward, cells were passaged when necessary.

Subsequently, hWJ-MSCs were detached and seeded on P(NIPAm-co-NIPMAm) and P(NIPAm-co-NIPMAm)/P3HT6S hydrogels that had been previously placed in a 24-well plate and sterilized under UV light for 30 min. The cell seeding density was 1×10^3 cells/cm². As a control condition, the same cell density was seeded on tissue culture plates (TCP). Samples were incubated and cultured at 37 °C and 5% CO_2. The medium was changed every 3 days.

2.7.2. Cell Viability. To assess the biocompatibility of P(NIPAm-co-NIPMAm) and P(NIPAm-co-NIPMAm)/P3HT6S hydrogels, samples were subjected to a colorimetric MTT [3-(4,5-dimethylthiazol-2-yl)-2,5-diphenyltetrazolium bromide] assay. Cell metabolic activity was measured by means of dehydrogenase enzymes, which reduce MTT yellow salt (3-(4,5-dimethylthiazolyl-2)−2,5-diphenyltetrazolium bromide) to NADP and NADPH. In detail, 50 μL of MTT solution (5 mg/mL in PBS) was added to each well. To dissolve the formazan crystals, 500 mL of MTT solubilization solution was added after a 2 h incubation. Lastly, the absorbance at 570 mm was measured by UV−vis spectroscopy (Thermo Scientific Multiscan FC). An increased or decreased cell number was recorded in the presence of a concomitant change in the amount of formazan formed, thus indicating the degree of cytotoxicity caused by the tested material. The cell viability of hWJ-MSCs cultured on P(NIPAm-co-NIPMAm) and P(NIPAm-co-NIPMAm)/P3HT6S hydrogels was investigated on the cultures for up to 7 days, with a middle time point set at day 3. Viability results were normalized to TCP control as relative percentages.

2.7.3. Immunocytochemical Assay. In order to further investigate the viability of the cells cultured on the P(NIPAm-co-NIPMAm)/P3HT6S hydrogel, cell immunocytochemical analysis was conducted on day 7 of culture. The expression of protease enzymes (i.e. caspases 3 and 8), which play a crucial role in cell apoptosis, and the expression of a cellular proliferation marker (i.e. Ki67) were evaluated. In detail, samples in 24-well culture plates were rinsed in 0.1 M PBS and fixed with 4% buffered paraformaldehyde (pH 7.4) for 10 min. Then, hWJ-MSCs were permeabilized with 0.025% Triton X-100 (Sigma-Aldrich) and incubated with a blocking mixture containing 10% normal goat serum (Invitrogen) in PBS for 60 min at room temperature with the aim of reducing non-specific background staining. Afterward, hWJ-MSCs were washed with PBS (3 × 5 min) and incubated overnight in a humid chamber at 4 °C in a solution of primary antibodies for caspase 3, caspase 8, and Ki67. Subsequently, hWJ-MSCs were rewashed in PBS (3 × 5 min) and incubated in a solution of secondary antibodies (Alexa Fluor 488 or Alexa Fluor 555, Jackson Immuno Research Labs) for 1 h, in the dark, at room temperature. The working dilution of primary and secondary antibodies was 1:500. After incubation, hWJ-MSCs were rewashed in PBS (3 × 5 min) and then mounted using a mounting medium with DAPI (Santa Cruz Biotechnology, Dallas, Texas, USA). Samples were imaged using a confocal microscope (Olympus BX51).

2.8. Neural Progenitor Cell Culture. *2.8.1. Neural Progenitor Cell Isolation and Culture.* NPCs of postnatal-day-4 C57BL6 mice were isolated from the sub-ventricular zone (SVZ) and cultured according to Fiorelli *et al.*[59] Briefly, postnatal-day-4 mice were anesthetized in ice and, after brain extraction, the rostral Sub-

Ventricular Zone was micro-dissected. The tissue was digested in TripleX (Invitrogen) at 37 °C in the presence of 0.01% DNAseI and manually triturated with fire-polished glass Pasteur pipettes of decreasing diameters. Single-cell suspensions were then filtered through a 40 μm cell strainer (BD Falcon). Subsequently, 10×10^4 viable cells were plated in 2 cm Petri dishes in non-attachment conditions and cultured in 2 mL of DMEM/F12 medium supplemented with N2 (Gibco), 20 ng/mL of epidermal growth factor (EGF, Peprotech), 20 ng/mL of fibroblast growth factor 2 (FGF2, Peprotech), and antibiotic/antimycotic. Progenitor cells formed floating neurospheres after 7 days. Passaging was then performed at a density of 50 cells/μL every 4−7 days.

P(NIPAm-co-NIPMAm) and P(NIPAm-co-NIPMAm)/P3HT6S hydrogels were prepared in 1 cm-wide 4-well Petri dishes (Greiner bio-one) and sterilized under UV light for 30 min.

Hydrogels were additionally coated with 0.01% polylysine for 12 h at room temperature and 0.001% laminin for 2 h at 37 °C.

Neurospheres were manually selected when their mean diameter reached 150 +/− 50 μm, seeded on the hydrogel surfaces, and cultured in a Neurobasal A medium supplemented with B27 (Gibco), Glutamax 0.5 mM, and antibiotics/antimycotic. Upon attachment onto the substrates, NPCs migrated radially and differentiated into mixed neural/glial cultures. The differentiation medium was refreshed every second day.

2.8.2. Immunofluorescent Staining and Imaging. Cells were fixed in 4% paraformaldehyde at 3 and 10 d.v.i. before performing immunofluorescence assays. After thorough washing in 0.1 M phosphate buffer at pH 7.4 (PB), non-specific epitopes were blocked in PB modified with 0.4% Triton-X and 10% inactivated goat serum (Gibco) for 30 min at room temperature. Primary antibodies (chicken Anti-Map2 (Synaptic Systems) diluted 1:1000 and mouse anti-GFAP (Millipore, clone GA5) diluted 1:500) were diluted in PB-0.4% Triton-X with 2% goat serum and applied onto the cells overnight at 4 °C. After washing, samples were incubated for 2 h at 4 °C in a secondary antibody solution including goat anti-mouse Alexa 568 and goat anti-chicken Alexa 488 (Jackson) diluted 1:2000 in PB-0.4% Triton-X with 2% goat serum. Nuclear counterstaining was performed with DAPI diluted 1:500. Coverslips were mounted using Mowiol.

Immunofluorescence assays were imaged using a Leica SPE laser scanning microscope with 20× objective. For quantification, in three independent experiments, images from at least four fields per sample were selected. Images were analyzed using ImageJ. Both the manual quantification of the number of cells/type and the morphological analysis of MAP2+ neurons, including dendritic length and complexity of ramification (i.e., number of nodes), were performed in blind.

2.9. Light-Based Stereolithographic Semi-IPN Hydrogel 3D Printing. *2.9.1. 3D Laser Printing of the P(NIPAm-co-NIPMAm)/P3HT6S Hydrogel.* 2,4,6-Trimethylbenzoyl-diphenyl phosphine oxide (Omnirad TPO, IGM resins) photoinitiator was added to the precursor solution (5% wt of the final polymer composition). Such composition allows a good printability of the thiophene-doped ink, notwithstanding the residual absorption of P3HT6S at the printing wavelength.[46] The experimental system used for laser printing includes a UV laser source with an emission wavelength of 405 nm and a maximum power of 1 mW (measured at the sample position). The laser is coupled with an inverted microscope and focused on the sample with a 20× objective (numerical aperture, NA = 0.75), which can be translated axially (parallel to the laser propagation axis) with a sub-micrometric resolution. The laser spot was scanned in the sample plane by a galvanometer mirror with a typical scanning speed in the range of 0.1−1 of mm s⁻¹. To prevent the significant evaporation of water during the printing process, the (NIPAm-co-NIPMAm)/P3HT6S hydrogel precursor was loaded into a cell with an area of 1 × 1 cm² and a 5 mm thickness. The cell was created by placing a polydimethylsiloxane (PDMS, Dow Corning) slab with a central hole in conformal contact with a glass substrate, in order to define the vertical walls (PDMS) and cell-substrate (glass). After loading the precursor solution, the cell was sealed with a glass coverslip over the PDMS slab. The PDMS slab was created using a mixture of base and curing agents with a 10:1 ratio, which was polymerized at room temperature.
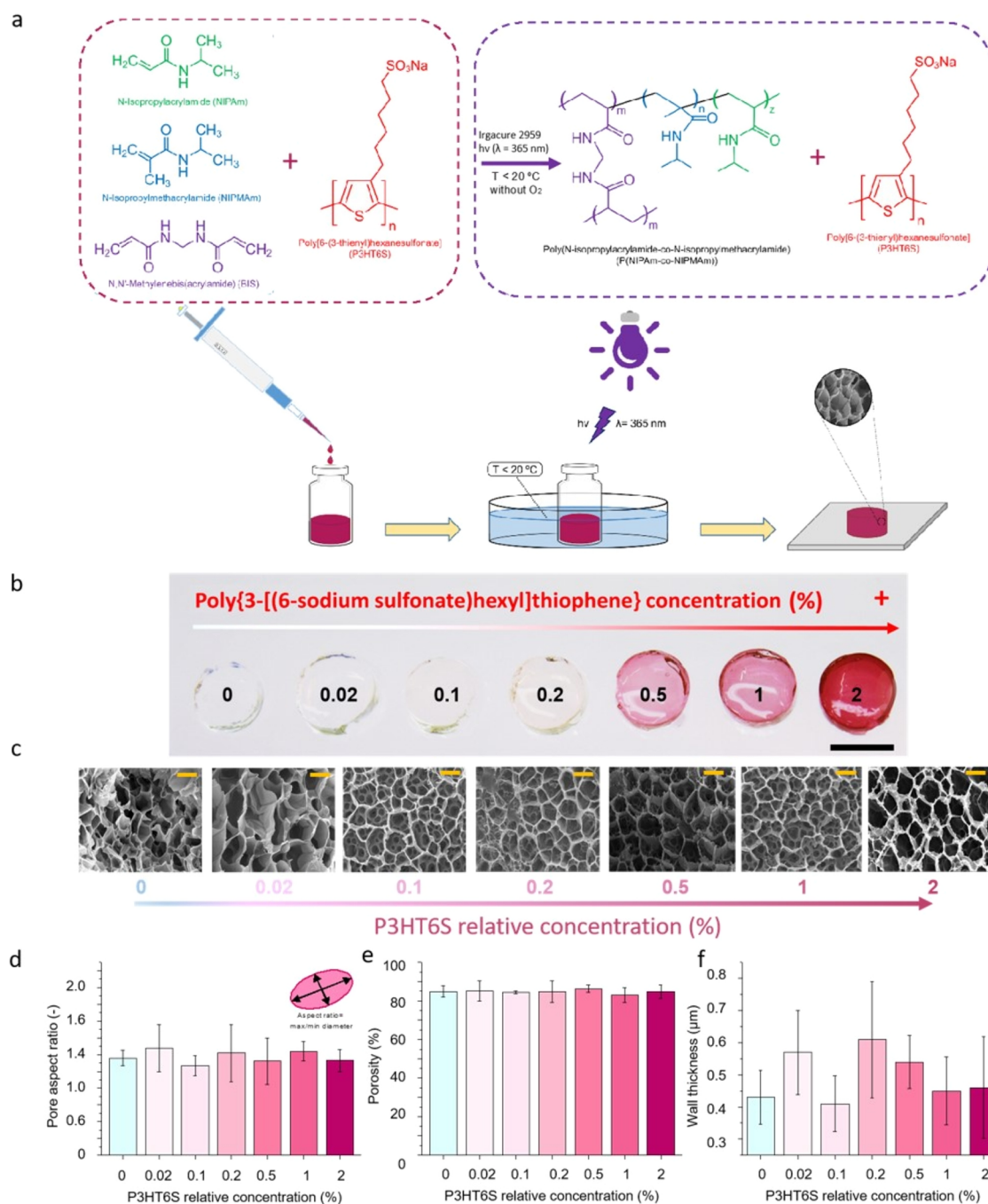
Figure 1. Production and morphological properties of P(NIPAm-*co*-NIPMAm) and P(NIPAm-*co*-NIPMAm)/P3HT6S hydrogels. (a) Schematic representation of P(NIPAm-*co*-NIPMAm)/P3HT6S hydrogel fabrication. The P(NIPAm-*co*-NIPMAm)/P3HT6S hydrogel was developed by mixing P3HT6S, NIPAm, and NIPMAm in the presence of a cross-linker (BIS) and photoinitiator (Irgacure). Subsequently, the hydrogel precursor solution was degassed and exposed to UV light in a cold environment to form the cross-linked P(NIPAm-*co*-NIPMAm)/P3HT6S hydrogel. (b, c) Images of P(NIPAm-*co*-NIPMAm) hydrogels with increasing P3HT6S concentrations: (b) macroscopic images. Scale bar: 10 mm; (c) FE-SEM images. Scale bars: 20 μm. (d−f) Morphological characteristics of P(NIPAm-*co*-NIPMAm) hydrogels with increasing P3HT6S concentrations: pore aspect ratio (d), porosity (e) and wall thickness (f), showing the similar morphology of the different hydrogel conditions tested.

2.9.2. Morphological Characteristics of Hydrogel Printed Structures. The printed P(NIPAm-*co*-NIPMAm)/P3HT6S hydrogel structures were subjected to microscopic imaging using an upright microscope (BX51, Olympus) with a Tungsten lamp as the illumination source. In addition, samples were imaged by confocal microscopy, measuring the maps of the incident laser intensity transmitted by the printed objects. This analysis was conducted using an inverted microscope equipped with a confocal laser scanning head (FV1000, Olympus). Samples were excited by a diode laser (emission wavelength 405 nm), which was focused onto the sample surface with a 10× objective with NA = 0.4. The intensity of the laser transmitted by the sample was measured by a photomultiplier.

2.10. Statistical Analysis. Measurements were performed in triplicate, unless specified. Data are expressed as mean values ± standard deviation. A one-way ANOVA test was conducted, and significant differences were reported when $p \leq 0.05$. More specifically, statistically significant values are shown as *$p \leq 0.05$, **$p \leq 0.01$, ***$p \leq 0.001$, and ****$p \leq 0.0001$.
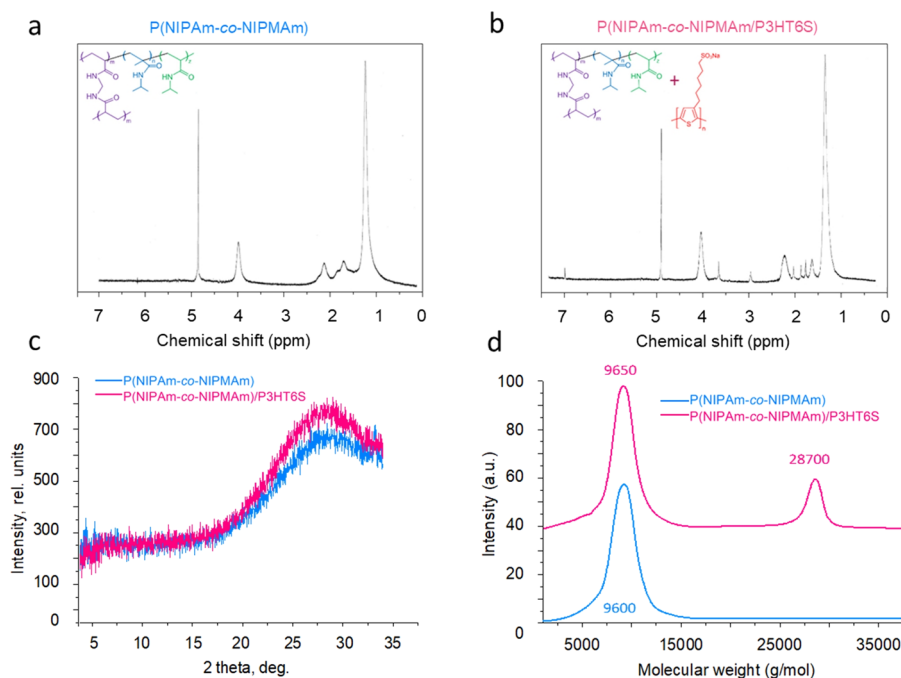
Figure 2. Chemical characteristics of the developed materials. (a) NMR graph of the soluble fraction of the P(NIPAm-*co*-NIPMAm) hydrogel, illustrating the characteristic peaks of each component: ^{1}H NMR (D$_2$O, ppm): δ 3.87 (1H, bm), 2.02 (1H, bm), 1.53 (2H, bm), 1.11 (6H, bm). (b) NMR graph of the soluble fraction of the P(NIPAm-*co*-NIPMAm)/P3HT6S hydrogel, illustrating the characteristic peaks of each component: ^{1}H NMR (D2O, ppm): δ 7.01 (s), 3.90 (bm), 3.48 (m), 2.79 (m), 2.02 (bm), 1.84 (m), 1.73 (m), 1.54 (bm), 1.43 (m), 1.05 (m). (c) XRD curves of P(NIPAm-*co*-NIPMAm) and P(NIPAm-*co*-NIPMAm)/P3HT6S hydrogels, showing the characteristic amorphous diffraction peak. (d) GPC curves of the soluble fraction of P(NIPAm-*co*-NIPMAm) and P(NIPAm-*co*-NIPMAm)/P3HT6S hydrogels, showing the presence of a second peak for the composite hydrogel.

3. RESULTS AND DISCUSSION

For the design of scaffolds for neural tissue engineering, it is of crucial importance to develop a soft conducting material capable of promoting neural signaling and tissue repair while ensuring the matching of brain mechanical properties.[60,61]

In this work, we propose a soft conductive polymer hydrogel made of polyacrylamide with the addition of polythiophene, in order to provide the system with good electrical properties. To achieve this formulation, polythiophene was synthesized by introducing ionic pendant groups into flexible side chains, thus obtaining a water-soluble P3HT6S (Figure S2). After dissolving P3HT6S in water, NIPAm-*co*-NIPMAm components were added, forming the hydrogel precursor solution. The final platform was developed by synthesizing the P(NIPAm-*co*-NIPMAm) hydrogel interpenetrated with P3HT6S chains by the exposure to UV light in a cold environment, resulting in a semi-IPN (Figure 1a). Keeping the temperature below 20 °C during the fabrication process is crucial to avoid exceeding the lower critical solution temperature (LCST) of the PNIPAm-based system, thus avoiding polymer network deformations and inhomogeneity.

In this study, several P(NIPAm-*co*-NIPMAm)/P3HT6S hybrid hydrogels were fabricated using different P3HT6S concentrations to evaluate the effect of P3HT6S addition into the P(NIPAm-*co*-NIPMAm) hydrogel network (Tables S1 and S2). Concentrations of P3HT6S greater than 2% were also tested (Figure S3). However, in the case of high concentrations, the P3HT6S solubility in the hydrogel precursor solution was not optimal and aggregation phenomena were observed; thus, the P(NIPAm-*co*-NIPMAm)/P3HT6S hydrogel with 2% of P3HT6S proved to be the highest P3HT6S-concentrated

homogeneous hydrogel achievable. The incremental addition of P3HT6S caused visible color changes. Indeed, the brownish color of P3HT6S caused darker red shades in the hydrogel in proportion to the P3HT6S concentration, thus obtaining different colored hydrogel structures ranging from transparent to red (Figure 1b).

The morphology of P(NIPAm-*co*-NIPMAm) hydrogel formulations with increasing concentrations of P3HT6S was investigated by FE-SEM (Figure 1c) to verify that the P3HT6S-modified P(NIPAm-*co*-NIPMAm) hydrogel maintained the suitable properties of the pristine P(NIPAm-*co*-NIPMAm) hydrogel for tissue engineering purposes. The analysis of FE-SEM images showed that the addition of P3HT6S did not negatively affect the morphological characteristics of hydrogels in terms of the pore aspect ratio (Figure 1d), porosity (Figure 1e), and wall thickness (Figure 1f), which did not appear significantly different for all the P3HT6S concentrations tested. All samples had an open porosity of around 85%, showing pores with a polygonal shape. For these reasons, no adverse effects in terms of physical or structural properties related to the addition of up to 2% P3HT6S into the P(NIPAm-*co*-NIPMAm) hydrogel formulation are expected.

Since the incremental addition of P3HT6S evidenced no structural or morphological changes, the highest P3HT6S-concentrated P(NIPAm-*co*-NIPMAm)/P3HT6S hydrogel (2%) was selected for further tests.

The chemical characteristics of P(NIPAm-*co*-NIPMAm) and P(NIPAm-*co*-NIPMAm)/P3HT6S hydrogels were thoroughly studied.

^{1}H NMR of the soluble fraction of the P(NIPAm-*co*-NIPMAm) hydrogel (Figure 2a), recorded in D$_2$O, showed two signals at 2.02 and 1.53 ppm, which can be attributed to the
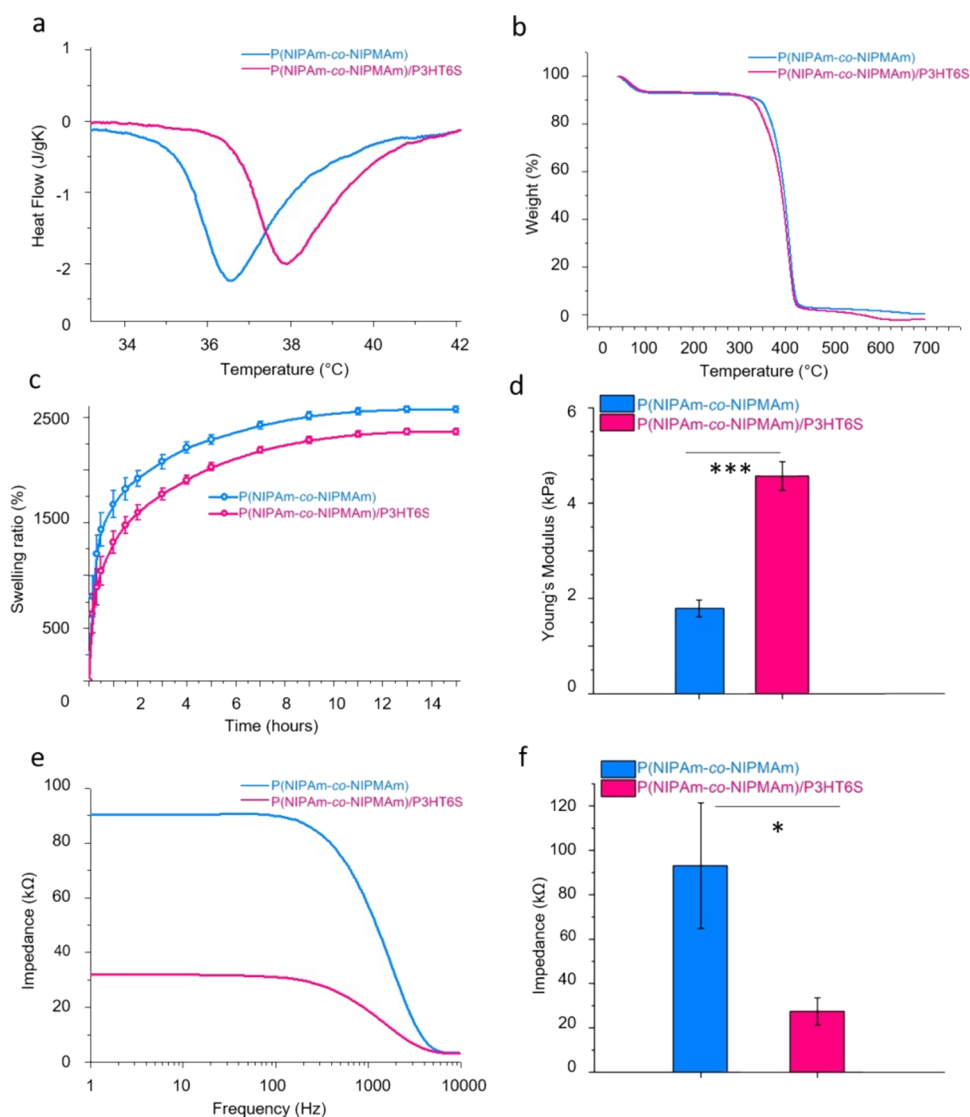
Figure 3. Physical characteristics of P(NIPAm-*co*-NIPMAm) and P(NIPAm-*co*-NIPMAm)/P3HT6S hydrogels. (a) DSC curves of hydrated samples, showing the shift in LCST of the P(NIPAm-*co*-NIPMAm)/P3HT6S hydrogel. (b) TGA curves showing the thermal stability of the tested hydrogels. (c) Swelling ratio showing the lower ability of P(NIPAm-*co*-NIPMAm)/P3HT6S hydrogel to swell in an aqueous medium. (d) Mechanical characteristics, showing the higher properties of the P(NIPAm-*co*-NIPMAm)/P3HT6S hydrogel in terms of Young's Modulus. (e, f) Hydrogel electrical properties: impedance curves (e) and values at biomedically significant frequencies (f), highlighting the lower impedance values of the P(NIPAm-*co*-NIPMAm)/P3HT6S hydrogel at relevant biomedical frequencies. Significant differences are reported when $p \leq 0.05$, *$p < 0.05$, **$p < 0.01$, ***$p < 0.001$, and ****$p < 0.0001$.

methinic and methylenic protons, respectively, of the main chain. Moreover, two other signals at 3.87 and 1.11 ppm were recorded due to the methinic and methylic protons, respectively, of the side chain. The sharp peak at 4.80 ppm is related to the solvent. The recorded signals are poorly resolved. This can be attributed to the copolymer's relatively high molecular weight and the hydrogel's cross-linked structure that tends to form a rather viscous solution in the NMR probe. The NMR spectrum of the soluble fraction of the P(NIPAm-*co*-NIPMAm)/P3HT6S hydrogel physical blend showed both hydrogel and P3HT6S signals (Figure 2b). In particular, the signals of the latter can be found at 7.01 (H$_4$-thiophene), 3.48 ($-CH_2SO_3-$), 2.79 ($-CH_2Th$), 1.84 ($-CH_2CH_2SO_3-$), 1.73 ($-CH_2CH_2CH_2SO_3-$), and 1.43 ppm ($-CH_2-$). The observed resonances are in good agreement with those recorded for P3HT6S (Figure S4a).

Moreover, the X-ray diffractograms (XRD) of P(NIPAm-*co*-NIPMAm) and P(NIPAm-*co*-NIPMAm)/P3HT6S hydrogels were analyzed. A typical amorphous diffraction peak was observed for both samples, indicating the presence of amorphous phases in polymer hydrogels (Figure 2c).

Furthermore, GPC was performed to evaluate the molecular weights of the soluble fraction of P(NIPAm-*co*-NIPMAm) and P(NIPAm-*co*-NIPMAm)/P3HT6S hydrogels (Figure 2d). A first peak was detected at ∼9600 g/mol for the soluble fraction of P(NIPAm-*co*-NIPMAm) hydrogel with an Mw/Mn of 1.29. On the other hand, the soluble fraction of the P(NIPAm-*co*-NIPMAm)/P3HT6S hydrogel also showed a second peak at ∼28,700 and an Mw/Mn of 1.28, which may be attributed to the P3HT6S component, as reported in the GPC curve of the pristine P3HT6S polymer (Figure S4b).

LCST values of P(NIPAm-*co*-NIPMAm) and P(NIPAm-*co*-NIPMAm)/P3HT6S hydrogels were evaluated by DSC to
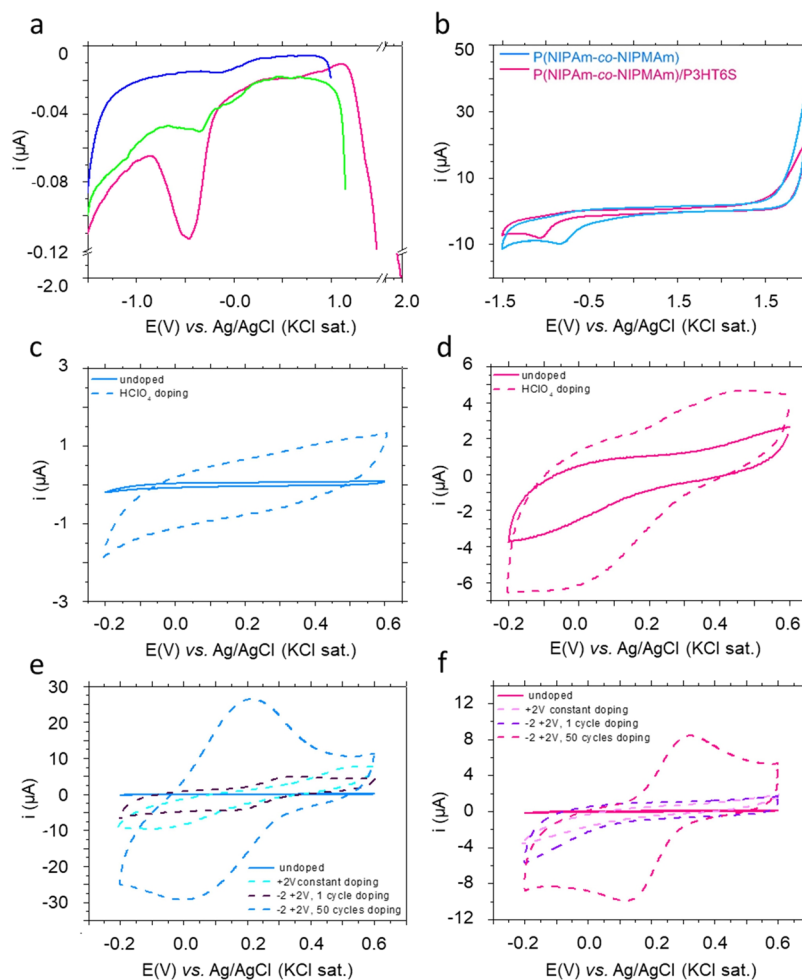
G

Figure 4. Cyclic voltammogram of hydrogel-modified GCEs. (a) Comparison of differential pulse voltammograms showing the initial potential dependence on the reduction peak. DPV conditions: initial potential +1 V (blue line), +1.5 V (green line), +2 V (pink line), end potential −1.5 V. (b) CV of the P(NIPAm-*co*-NIPMAm) hydrogel vs P(NIPAm-*co*-NIPMAm)/P3HT6S hydrogel showing the shifting of the reduction peak to more negative potentials in the presence of P3HT6S. (c, d) Comparison of the chemically doped (dash line) and undoped (solid line) P(NIPAm-*co*-NIPMAm) (c) and P(NIPAm-*co*-NIPMAm)/P3HT6S (d) hydrogels. (e, f) Comparison of electrochemically doped (dash line) and undoped (solid line) P(NIPAm-*co*-NIPMAm) (e) and P(NIPAm-*co*-NIPMAm)/P3HT6S (f) hydrogels, showing an effective doping in the case of 50 cycles of sweeping potential between −2 and + 2 V in the presence of P3HT6S. Scan rate, 0.1 V/s.

determine the effects of P3HT6S addition on the thermal properties of the hybrid material. Data presented in Figure 3a show increased LCST values in the presence of P3HT6S from 36.5 to 38 °C for P(NIPAm-*co*-NIPMAm) and P(NIPAm-*co*-NIPMAm)/P3HT6S hydrogels, respectively. This is most probably due to the presence of a second polymer with different thermal properties.[62] The glass transition temperature was measured to be around 157 °C without a significant difference between the tested hydrogel compositions (Figure S5a).

Furthermore, TGA showed that P(NIPAm-*co*-NIPMAm) and P(NIPAm-*co*-NIPMAm)/P3HT6S hydrogels degraded during the heating process up to 700 °C (Figure 3b). In the first part of the heating process (to approximately 150 °C), most of the sample water content evaporated. In the 250−500 °C temperature range, the degradation step was observed: ∼90% of the sample mass was degraded in both P(NIPAm-*co*-NIPMAm) and P(NIPAm-*co*-NIPMAm)/P3HT6S hydrogels. An excellent thermal stability was reported for each hydrogel condition.

Moreover, the swelling properties of P(NIPAm-*co*-NIPMAm) and P(NIPAm-*co*-NIPMAm)/P3HT6S hydrogels were evaluated by incubating the samples in an aqueous solution and assessing the water absorption. The results shown in Figure 3c

evidence that both P(NIPAm-*co*-NIPMAm) and P(NIPAm-*co*-NIPMAm)/P3HT6S hydrogels swelled remarkably (up to ∼2000%) due to their intrinsic water absorption ability. However, P(NIPAm-*co*-NIPMAm)/P3HT6S hydrogels swelled less than P(NIPAm-*co*-NIPMAm) hydrogel. This is probably due to the different polarity of the tested conditions, which led to a lower water-absorbing capacity of the hybrid hydrogel.

Additionally, the mechanical properties of the samples were also evaluated by means of nanoindentation. The data showed significantly higher mechanical properties of the P(NIPAm-*co*-NIPMAm)/P3HT6S hydrogel compared to the P(NIPAm-*co*-NIPMAm) hydrogel in terms of Young's Modulus (Figure 3d). Values of ∼4.6 +/−0.3 kPa were detected for the P(NIPAm-*co*-NIPMAm)/P3HT6S hydrogel, which can well match the mechanical properties of the brain slice (1−10 kPa), thus permitting an optimal mechanical integration of the material into the brain tissue.[16]

Furthermore, electrical tests were performed on P(NIPAm-*co*-NIPMAm) and P(NIPAm-*co*-NIPMAm)/P3HT6S hydrogels to evaluate the effect of P3HT6S addition on the electrical properties of the final materials. Results demonstrate the significantly lower electrical impedance of P(NIPAm-*co*-
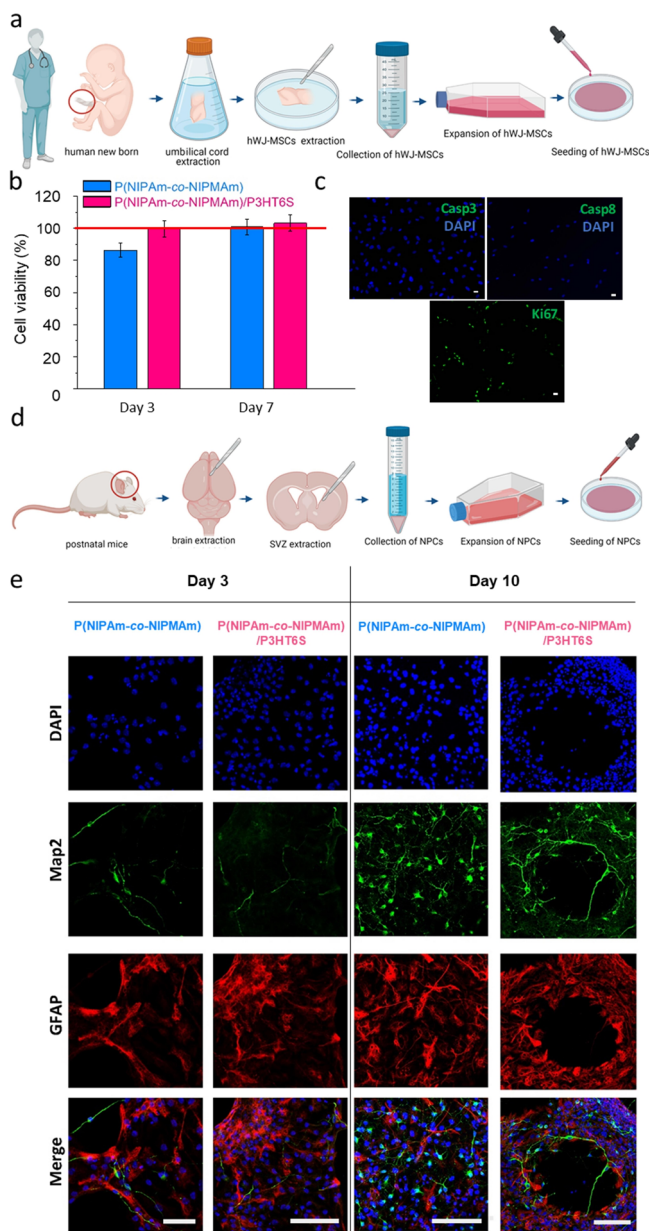
Figure 5. *In vitro* cell studies on P(NIPAm-*co*-NIPMAm) and P(NIPAm-*co*-NIPMAm)/P3HT6S hydrogels. (a−c) hWJ-MSC culture: (a) scheme of cell isolation from human umbilical cord. Created with BioRender.com; (b) high cell viability was detected for both hydrogel conditions at each time point tested. Data are normalized to control condition (TCP, red line) and expressed as relative percentages; (c) confocal images of Casp3, Casp8, and Ki67 (green) expressed by hWJ-MSCs cultured on the P(NIPAm-*co*-NIPMAm)/P3HT6S hydrogel showing the absence of apoptosis markers (i.e. Casp3 and Casp8), while illustrating the presence of the Ki67 proliferation marker (green). DAPI nuclear stain (blue). Scale bars: 10 μm. (d, e) NPC culture: (d) scheme of cell isolation from mice SVZ. Created with BioRender.com; (e) confocal images of neurospheres cultured on the hydrogel substrates at 3 and 10 d.v.i, showing the maturation of Map2-positive neurons (green) and GFAP-positive astrocytes (red) during the culture time. DAPI nuclear staining (blue). Scale bars: 100 μm.

NIPMAm)/P3HT6S hydrogels, as revealed by lower values of impedance measured at the most relevant frequencies from the biomedical point of view (i.e., 10 Hz) (Figure 3e,f). The higher electrical properties of the hybrid hydrogel are related to the

presence of the P3HT6S conductive polymer and promoted by the efficient integration of P3HT6S into the P(NIPAm-*co*-NIPMAm) hydrogel network. The improved electrical properties of the P(NIPAm-*co*-NIPMAm)/P3HT6S hydrogel make it a promising candidate for neural tissue engineering applications, potentially promoting the conduction of neural electrical signals in physiological environments.

The cross-linked P(NIPAm-*co*-NIPMAm) and P(NIPAm-*co*-NIPMAm)/P3HT6S hydrogels were washed several times by immersion in water to remove any unreacted material. Figure S5b shows that both tested materials successfully released around 100% photoinitiator within 2 h of incubation in an aqueous medium, thus preventing the presence of toxic molecules.

Afterward, the electrochemical properties of P(NIPAm-*co*-NIPMAm) and P(NIPAm-*co*-NIPMAm)/P3HT6S hydrogels were investigated by CV and DPV.[54] In scans between +2 and −2 V, a peak at approximately −0.7 V was detected (Figure S5c). This peak may be attributed to O_2, in case the solution was not deoxygenated (Figure 4a). The current peak did not increase when the buffer solution was purged with dioxygen, and therefore it was attributed to the reduction of a product formed at positive potentials greater than +1.5 V. Indeed, if the hydrogel was not overoxidized above +1.5 V, the peak disappeared (Figure 4a). On the other hand, another peak appeared at approximately − 0.5 V, and its height depended on the value of the initial potential. If a strongly positive initial potential was selected (approximately + 2 V), the reduction peak at approximately −0.5 V appeared to be well developed. This was again attributed to the reduction of hydrogel precursor overoxidation products (Figure 4b). Moreover, the presence of P3HT6S leads to a shift in this product reduction toward negative potentials (Figure 4b). Conversely, choosing +1 V as the initial potential leads to a completely flat voltammetric curve (Figure 4a). In other words, the scanning potential in the range of +1 to −1.4 V did not affect hydrogel-modified GCEs, and no redox signals appeared in the voltammogram. However, the hydrogel film was not conductive under such conditions.

In order to improve the conductivity of the hydrogel film, two doping methods were tested: (i) chemical doping by immersion in $HClO_4$ solution and (ii) electrochemical doping by exposure to highly positive potentials. The first approach relies on doping hydrogel-modified electrodes by the exposure to an $HClO_4$ solution.[63] The doping effect was monitored in an FCN solution by recording the cyclic voltammogram and determining the reduction and oxidation peaks potentials. The peak couple appeared at approximately 250 mV versus Ag/AgCl (KCl sat.). Results reported in Figure 4c,d make it possible to visualize the barely visible peaks in both $HClO_4$-doped and undoped systems. In the $HClO_4$-doped system, the background current has a large capacitive component. This may be considered interesting for supercapacitor applications but not very convenient from the viewpoint of determination of low concentrations of analytes. For this reason, chemical doping using $HClO_4$ does not appear very promising in the case of P(NIPAm-*co*-NIPMAm) and P(NIPAm-*co*-NIPMAm)/P3HT6S hydrogel-modified electrodes. Furthermore, degradation phenomena related to $HClO_4$ exposure may limit the application of this doping method to the targeted materials.

In the second approach, electrochemical doping was performed by first applying a + 2 V constant potential and then applying cyclic potential scans between −2 and + 2 V.[56] Figure 4e,f shows the characteristic FCN peaks at approximately
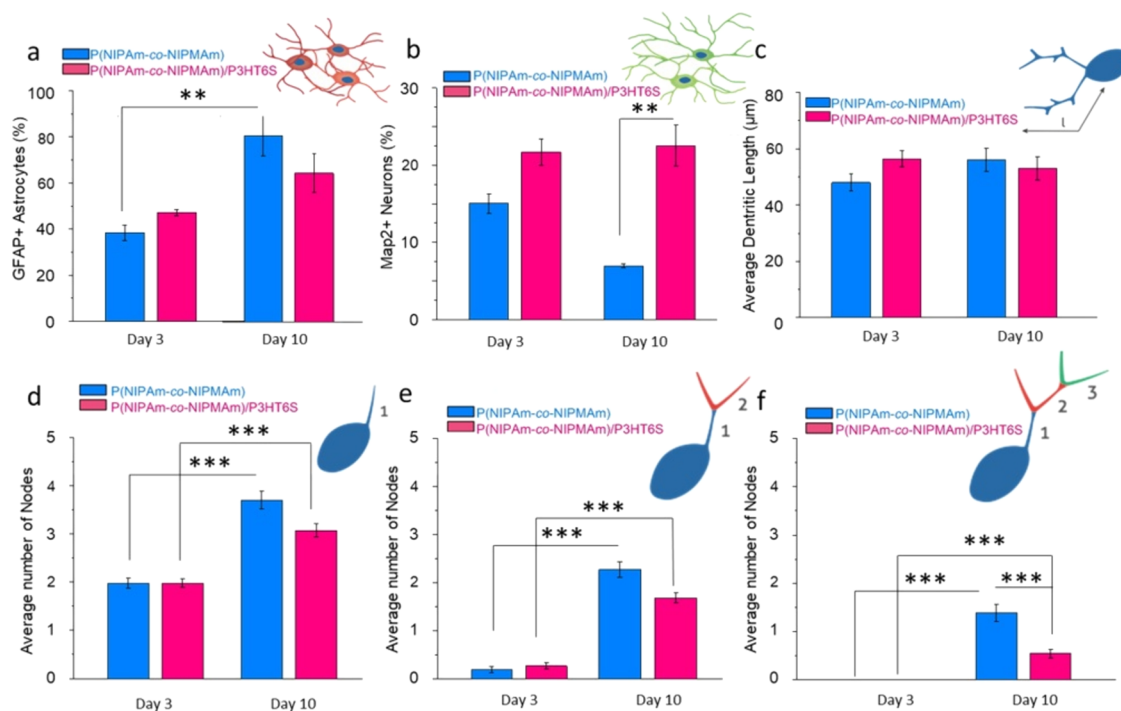
Figure 6. *In vitro* neuro-glial cell cultures on P(NIPAm-*co*-NIPMAm) and P(NIPAm-*co*-NIPMAm)/P3HT6S hydrogels: confocal image quantification. (a, b) Percentage of Map2+ stained neurons (a) and GFAP+ stained astrocytes (b) at 3 and 10 d.i.v. While the glial population was consistently increasing over time across conditions, the % of neurons decreased in the P(NIPAm-*co*-NIPMAm) hydrogel condition while remaining stable on the P(NIPAm-*co*-NIPMAm)/P3HT6S hydrogel. (c) Dendritic length at 3 and 10 d.i.v. (d–f) Arborization of neurons at 3 and 10 d.i.v., showing the number of first (d), second (e) and third (f) orders of nodes. At the early stages of culture, most of the neurons are uni- or bipolar. At 10 d.v.i. of culture, an increased complexity of arborization is observed by the appearance of third-order nodes in both hydrogel conditions. Significant differences are reported when $p \leq 0.05$, *$p < 0.05$, **$p < 0.01$, ***$p < 0.001$, and ****$p < 0.0001$.

250 mV versus Ag/AgCl (KCl sat.) Additionally, if the number of cycles between positive and negative potentials increased up to 50 cycles, the hydrogel-modified electrodes show a higher conductivity. In the case of the P3HT6S presence in the hydrogel coating, the peak couple corresponding to $[Fe(CN)_6]^{3-/4-}$ electrode processes was better developed and much more reversible, meaning that the film overoxidation pretreatment at +2 V and wide-range multiple potential scans improved the film's conductivity. Thus, the electrochemical doping by exposure to a highly positive voltage (i.e., cyclic potential scans between −2 and +2 V) facilitated the electrolyte penetration through the hydrogel film leading to the desired improved conductivity of the P(NIPAm-*co*-NIPMAm)/P3HT6S hydrogel and allowing to obtain reversible voltammograms of the electrochemical probes. Hence, our results reveal the improved conductivity of the system achieved when P3HT6S is introduced into the hydrogel formulation.

Control and optimization of the cell activity on hydrogels designed for tissue engineering purposes are crucial in many applications.[64] Human mesenchymal stem cells (hMSCs) are routinely used for cytotoxicity and viability evaluation of biomaterials.[65−67] More specifically, the assessment of hMSCs on P(NIPAm)-based materials has been fully evaluated in a previous study by Yang *et al.*[68] Authors reported viability, proliferation, and differentiation of hMSCs cultured on P(NIPAm)-based surfaces.[68] Moreover, the beneficial biological properties of polyacrylamide scaffolds were also demonstrated by Li and co-workers, revealing their potential application in peripheral nerve regeneration.[69]

Therefore, in this work, the biological response of P(NIPAm-*co*-NIPMAm) and P(NIPAm-*co*-NIPMAm)/P3HT6S hydro-gels was investigated by evaluating the viability and tendency of hWJ-MSCs to proliferate. hWJ-MSCs were isolated from human umbilical cord, cultured, and expanded (Figure 5a).[57,58] Afterward, cells were seeded onto the samples and the possible hydrogel toxic effect on cell activity was determined by MTT assay. Figure 5b shows that the hWJ-MSC viability percentage increased during the culture time for all analyzed materials, thus evidencing that P(NIPAm-*co*-NIPMAm) and P(NIPAm-*co*-NIPMAm)/P3HT6S hydrogels can support cell proliferation without any toxicity. To confirm this result, the expression of apoptosis and proliferation markers of hWJ-MSCs cultured on the P(NIPAm-*co*-NIPMAm)/P3HT6S hydrogel was measured. The expression of apoptosis markers (e.g., caspase 3 and caspase 8), which play essential roles in programmed cell death (including apoptosis, pyroptosis, and necroptosis) and inflammation, was not detected, while a high expression of the proliferation marker Ki67 was observed (Figure 5c). Data confirm the suitability of the proposed P(NIPAm-*co*-NIPMAm)/P3HT6S hydrogel platform for cell culture and proliferation and proved its biocompatibility.

To assess the proposed hydrogel platform compatibility to neural tissue, NPCs were isolated from brain SVZ of postnatal mice (Figure 5d) and cultured as floating neurospheres.[59,70] Mature spheres were seeded on P(NIPAm-*co*-NIPMAm) and P(NIPAm-*co*-NIPMAm)/P3HT6S hydrogels to investigate NPC differentiation into neural and glial lineage. Upon seeding, neurospheres (Figure S6a) quickly adhered to the substrate, while the radial migration of NPCs could be visualized 1 h after plating (Figure S6b). Single cells migrated radially from the center of the sphere (Figure S6c), while gradually differentiated and generated a network of MAP-2 positive neurons supported
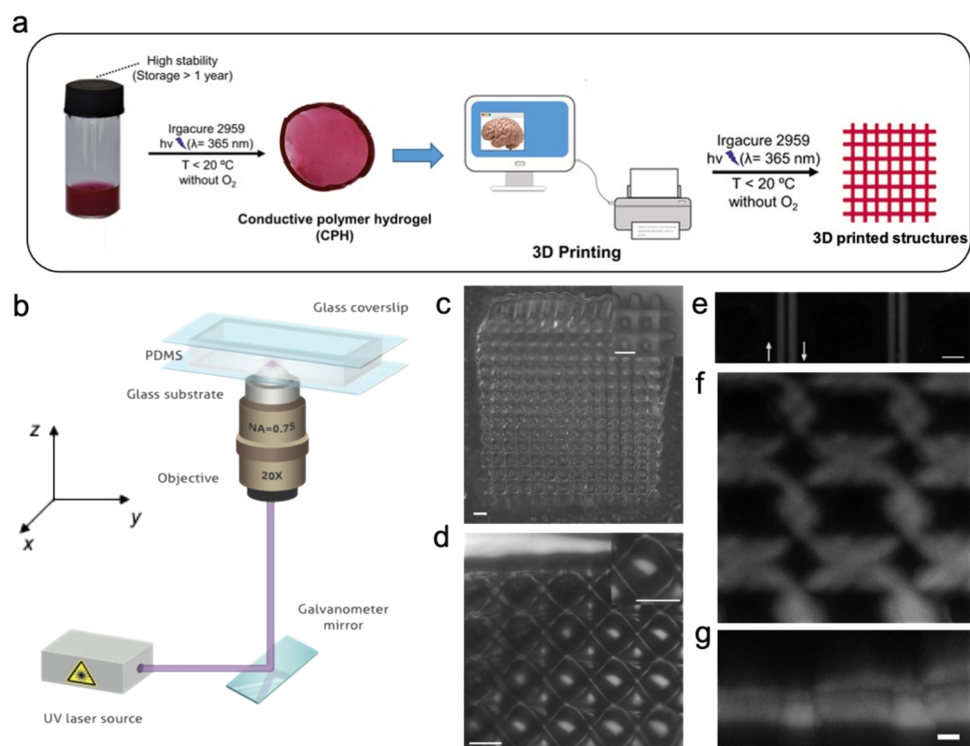
Figure 7. Laser 3D printing of the P(NIPAm-*co*-NIPMAm)/P3HT6S hydrogel. (a) Schematic representation of the 3D printing of the P(NIPAm-*co*-NIPMAm)/P3HT6S hydrogel. (b) Schematic representation of the laser printing setup. (c–g) Micrographs of the printed structures: hydrogel structures visualized by optical microscopy (c) and transmission laser microscopy (d). The insets show the magnified views of the printed objects. Scale bars: 50 μm; (e) laser confocal microscopy of single lines printed by scanning the laser used for polymerization along opposite directions, which are highlighted by arrows. Scale bar 10 μm; (f–g) x–y and corresponding x–z view of a laser-printed sample as imaged by z-stack laser confocal microscopy. Scale bar: 10 μm

by GFAP positive astrocytes (Figure 5e and Figure S6d). The phenotypical analysis revealed that at 3 d.i.v., 40% viable cells differentiated in astrocytes with no difference between substrates (Figure 6a). On the other hand, NPCs cultured on the P(NIPAm-*co*-NIPMAm)/P3HT6S hydrogel showed a significantly higher neural differentiation compared to the P(NIPAm-*co*-NIPMAm) hydrogel condition (∼20 vs 15%, respectively) (Figure 6b). Interestingly, the percentage of neural cells over the total population significantly decreased over time in the P(NIPAm-*co*-NIPMAm) hydrogel culture, while on the P(NIPAm-*co*-NIPMAm)/P3HT6S hydrogel substrate, it remained stable. At 10 d.i.v., neurons and astrocytes were 10 and 90% of the viable cells in the P(NIPAm-*co*-NIPMAm) hydrogel, while their numbers were 20 and 80% in the P(NIPAm-*co*-NIPMAm)/P3HT6S hydrogel culture, respectively. Overall, these data suggest that the conductive hydrogel was more supportive for neuronal differentiation and survival.

To investigate potential differences in neuronal maturation, a morphological analysis of MAP2+ neurons was performed by measuring the dendritic length and complexity of ramification. No differences in the dendritic length were visualized between hydrogel conditions (Figure 6c). The dendritic complexity was subsequently measured by counting the number of arborization nodes of the first, second, and third degrees. At 3 d.i.v., the vast majority of neurons presented a bipolar morphology, with two primary dendrites and rare secondary arborizations (Figure 6d,e), without differences between the tested conditions. At 10 d.i.v., the number of nodes increased as the morphology became more complex (Figure 6e,f). Overall, the number of primary, secondary, and third-order nodes was significantly higher at 10

d.v.i. in each condition compared to 3 d.i.v., showing that the proposed hydrogel supports neuronal survival and differentiation (Figure 6d–f).

3.1. Outlook: 3D Laser Printing. Thanks to the relatively simple cross-linking method, the P(NIPAm-*co*-NIPMAm)/P3HT6S hydrogel formulation has a potential for use as ink in 3D printing applications.[71,72] Indeed, the exposure of the hydrogel precursor solution to UV light in a cold and degassed environment produces a substance suitable for the 3D custom-printing of complex hybrid hydrogel structures (Figure 7a).

Hydrogel printability was assessed by using a custom-made laser printing setup (Figure 7b). For this purpose, the precursor solution was loaded into a PDMS cell to prevent water evaporation during the printing process (Figure S7a,b), while a scanning focused laser was used for the creation of various patterns by locally polymerizing the precursor. Figure 7c–g shows representative micrographs of laser-printed structures, with a size of 600 × 600 μm^2, thus evidencing the successful fabrication of constructs made of the P(NIPAm-*co*-NIPMAm)/P3HT6S hydrogel. The spatial resolution of the printing process was evaluated by printing single features such as individual lines by scanning the laser along a straight path and opposite directions (Figure 7e).

The results show structures with feature size of the order of about 3 μm, which was a bit larger compared to the spot size of focused printing laser ($d_l \approx 1.22\lambda/NA = 0.66 \ \mu$m, where λ is the wavelength of the printing laser and NA is the numerical aperture of the objective, Figure 7a). A variation of the features size in the order of 10% is observed, evidencing a good reproducibility of the printing process. The used focusing optics

makes it possible to achieve structures with micrometric features and sizes as low as half a millimeter, suitable for printing micro-objects. Printed structures with larger sizes might be achieved either by scanning the sample holder by means of precision translation stages or using projection optics, as reported in recent works on stereolithography with hydrogels.[73,74] Overall, the possibility of producing micro-objects made of the P(NIPAm-*co*-NIPMAm)/P3HT6S hydrogel was demonstrated, revealing the potential of the proposed hydrogel precursor as a UV-curable 3D printing ink.

4. CONCLUSIONS

In this work, a novel conductive semi-IPN hydrogel made of P(NIPAm-*co*-NIPMAm) and P3HT6S was designed, synthesized, and characterized. In order to induce the successful formation of the hybrid hydrogel in an aqueous medium, a polythiophene chemical structure was modified and synthesized to ensure water solubility. The influence of P3HT6S concentration in the P(NIPAm-*co*-NIPMAm) hydrogel formulation was investigated in terms of morphological properties, showing comparable features of up to 2% P3HT6S concentrated hydrogels.

The chemical and thermal characterizations of the P(NIPAm-*co*-NIPMAm)/P3HT6S hydrogel were assessed. Significantly, improved electrical, electrochemical, and mechanical properties of the proposed hybrid hydrogel were achieved as compared to the pristine hydrogel formulation. Thus, the new platform potential for promoting the conduction of neural electrical signals in physiological environments and inducing an optimal mechanical integration in the brain tissue was evidenced. Additionally, the material's biocompatibility was demonstrated by a high viability rate of mesenchymal stem cells cultured in contact with the semi-IPN hydrogel. Furthermore, NPCs cultured on the P(NIPAm-*co*-NIPMAm)/P3HT6S hydrogel demonstrated that the hybrid hydrogel supported the survival of the two main cell types of the central nervous system (i.e., neurons and astrocytes). In particular, it was observed that this platform might promote the neural differentiation of cells, as evidenced by a more abundant quantity of neural cells on the P(NIPAm-*co*-NIPMAm)/P3HT6S hydrogel at late culture stages.

Lastly, the possible use of the hybrid hydrogel solution as a printing ink to fabricate 3D biomaterials with desirable morphological and handling properties was highlighted. Data demonstrate that the developed hybrid nanostructured hydrogel is useful and versatile for the design and fabrication of 3D-printed biomaterials. Taking into account all the results, the proposed soft, low-impedance, biocompatible, and 3D printable semi-IPN hydrogel denotes a promising potential for novel neural tissue engineering applications.

■ ASSOCIATED CONTENT

ⓈI Supporting Information

The Supporting Information is available free of charge at https://pubs.acs.org/doi/10.1021/acs.biomac.1c00524.

> Sample preparation for electrochemical analysis; synthesis scheme of P3HT6S; FE-SEM images of the P(NIPAm-*co*-NIPMAm) hydrogel with the addition of >2% P3HT6S; NMR of P3HT6S; GPC of P3HT6S; glass transition temperature of P(NIPAm-*co*-NIPMAm) and P(NIPAm-*co*-NIPMAm)/P3HT6S hydrogels; photoinitiator cumulative release from P(NIPAm-*co*-NIPMAm) and P-

(NIPAm-*co*-NIPMAm)/P3HT6S hydrogels; CV of P-(NIPAm-*co*-NIPMAm)/P3HT6S hydrogel-modified GCE; images of mouse SVZ-neurospheres floating in non-adherent cultures; images of the neurospheres seeded on P(NIPAm-*co*-NIPMAm)/P3HT6S hydrogels; images of the PDMS chamber used during 3D laser printing; and table of sample codes and detailed recipes (PDF)

■ AUTHOR INFORMATION

Corresponding Author

Filippo Pierini − *Department of Biosystems and Soft Matter, Institute of Fundamental Technological Research, Polish Academy of Sciences, Warsaw 02-106, Poland;* ⓞ orcid.org/0000-0002-6526-4141; Email: fpierini@ippt.pan.pl

Authors

Chiara Rinoldi − *Department of Biosystems and Soft Matter, Institute of Fundamental Technological Research, Polish Academy of Sciences, Warsaw 02-106, Poland*

Massimiliano Lanzi − *Department of Industrial Chemistry "Toso Montanari", Alma Mater Studiorum University of Bologna, Bologna 40136, Italy;* ⓞ orcid.org/0000-0002-2466-2813

Roberto Fiorelli − *Ivy Brain Tumor Center, Barrow Neurological Institute, Phoenix, Arizona 85013, United States*

Paweł Nakielski − *Department of Biosystems and Soft Matter, Institute of Fundamental Technological Research, Polish Academy of Sciences, Warsaw 02-106, Poland*

Krzysztof Zembrzycki − *Department of Biosystems and Soft Matter, Institute of Fundamental Technological Research, Polish Academy of Sciences, Warsaw 02-106, Poland*

Tomasz Kowalewski − *Department of Biosystems and Soft Matter, Institute of Fundamental Technological Research, Polish Academy of Sciences, Warsaw 02-106, Poland*

Olga Urbanek − *Laboratory of Polymers and Biomaterials, Institute of Fundamental Technological Research, Polish Academy of Sciences, Warsaw 02-106, Poland*

Valentina Grippo − *Faculty of Chemistry, University of Warsaw, Warsaw 02-093, Poland*

Katarzyna Jezierska-Woźniak − *Department of Neurology and Neurosurgery, University of Warmia and Mazury in Olsztyn, Olsztyn 11-041, Poland*

Wojciech Maksymowicz − *Department of Neurology and Neurosurgery, University of Warmia and Mazury in Olsztyn, Olsztyn 11-041, Poland*

Andrea Camposeo − *NEST, Istituto Nanoscienze CNR and Scuola Normale Superiore, Pisa 56127, Italy*

Renata Bilewicz − *Faculty of Chemistry, University of Warsaw, Warsaw 02-093, Poland;* ⓞ orcid.org/0000-0003-0058-3691

Dario Pisignano − *NEST, Istituto Nanoscienze CNR and Scuola Normale Superiore, Pisa 56127, Italy; Dipartimento di Fisica, Università di Pisa, I-56127 Pisa, Italy;* ⓞ orcid.org/0000-0003-3758-5199

Nader Sanai − *Ivy Brain Tumor Center, Barrow Neurological Institute, Phoenix, Arizona 85013, United States*

Complete contact information is available at:
https://pubs.acs.org/10.1021/acs.biomac.1c00524

Author Contributions

F.P. conceived and developed the idea. F.P., C.R., and P.N. synthesized the hydrogels. M.L. performed the polythiophene synthesis and characterization. O.U. performed the FE-SEM, DSC, and XRD measurements. T.A.K. performed the TGA analysis. F.P., V.G., and R.B. prepared the modified electrodes and carried out the voltammetry experiments. K.Z. carried out the electrical characterization. R.F. and N.S. conducted the NPC cultures, IHC, and confocal imaging. K.J.-W. and W.M. carried out the MSC studies. A.C. and D.P. fabricated and tested the printed structures. F.P. and C.R. acquired and processed data. C.R. and F.P. wrote the manuscript. All authors discussed the results and commented on the manuscript. F.P. supervised the project.

Notes

The authors declare no competing financial interest.

■ REFERENCES

(1) Fu, L.; Qu, Q.; Holze, R.; Kondratiev, V. V.; Wu, Y. Composites of Metal Oxides and Intrinsically Conducting Polymers as Supercapacitor Electrode Materials: The Best of Both Worlds? *J. Mater. Chem. A* **2019**, *7*, 14937−14970.

(2) Choi, S.; Lee, H.; Ghaffari, R.; Hyeon, T.; Kim, D.-H. Recent Advances in Flexible and Stretchable Bio-Electronic Devices Integrated with Nanomaterials. *Adv. Mater.* **2016**, *28*, 4203−4218.

(3) Zhou, R.; Li, P.; Fan, Z.; Du, D.; Ouyang, J. Stretchable Heaters with Composites of an Intrinsically Conductive Polymer, Reduced Graphene Oxide and an Elastomer for Wearable Thermotherapy. *J. Mater. Chem. C* **2017**, *5*, 1544−1551.

(4) Kayser, L. V.; Lipomi, D. J. Stretchable Conductive Polymers and Composites Based on PEDOT and PEDOT:PSS. *Adv. Mater.* **2019**, *31*, 1806133.

(5) Wang, X.; Gu, X.; Yuan, C.; Chen, S.; Zhang, P.; Zhang, T.; Yao, J.; Chen, F.; Chen, G. Evaluation of Biocompatibility of Polypyrrole *in Vitro* and *in Vivo*. *J. Biomed. Mater. Res., Part A* **2004**, *68A*, 411−422.

(6) Humpolicek, P.; Kasparkova, V.; Saha, P.; Stejskal, J. Biocompatibility of Polyaniline. *Synth. Met.* **2012**, *162*, 722−727.

(7) Javadi, M.; Gu, Q.; Naficy, S.; Farajikhah, S.; Crook, J. M.; Wallace, G. G.; Beirne, S.; Moulton, S. E. Conductive Tough Hydrogel for Bioapplications. *Macromol. Biosci.* **2018**, *18*, 1700270.

(8) Richardson-Burns, S. M.; Hendricks, J. L.; Foster, B.; Povlich, L. K.; Kim, D.-H.; Martin, D. C. Polymerization of the Conducting Polymer Poly(3,4-Ethylenedioxythiophene) (PEDOT) around Living Neural Cells. *Biomaterials* **2007**, *28*, 1539−1552.

(9) Hackett, A. J.; Malmström, J.; Travas-Sejdic, J. Functionalization of Conducting Polymers for Biointerface Applications. *Prog. Polym. Sci.* **2017**, *70*, 18−33.

(10) Green, R. A.; Lovell, N. H.; Poole-Warren, L. A. Impact of Co-Incorporating Laminin Peptide Dopants and Neurotrophic Growth Factors on Conducting Polymer Properties. *Acta Biomater.* **2010**, *6*, 63−71.

(11) Kenry; Liu, B. Recent Advances in Biodegradable Conducting Polymers and Their Biomedical Applications. *Biomacromolecules* **2018**, *19*, 1783−1803.

(12) Balint, R.; Cassidy, N. J.; Cartmell, S. H. Conductive Polymers : Towards a Smart Biomaterial for Tissue Engineering. *Acta Biomater.* **2014**, *10*, 2341−2353.

(13) Puiggalí-Jou, A.; del Valle, L. J.; Alemán, C. Drug Delivery Systems Based on Intrinsically Conducting Polymers. *J. Controlled Release* **2019**, *309*, 244−264.

(14) Idumah, C. I. Novel Trends in Conductive Polymeric Nanocomposites, and Bionanocomposites. *Synth. Met.* **2021**, *273*, 116674.

(15) Ding, H.; Zhong, M.; Kim, Y. J.; Pholpabu, P.; Balasubramanian, A.; Hui, C. M.; He, H.; Yang, H.; Matyjaszewski, K.; Bettinger, C. J. Biologically Derived Soft Conducting Hydrogels Using Heparin-Doped Polymer Networks. *ACS Nano* **2014**, *8*, 4348−4357.

(16) George, J.; Hsu, C.-C.; Nguyen, L. T. B.; Ye, H.; Cui, Z. Neural Tissue Engineering with Structured Hydrogels in CNS Models and Therapies. *Biotechnol. Adv.* **2020**, *42*, 107370.

(17) Lang, U.; Dual, J. Mechanical Properties of the Intrinsically Conductive Polymer Poly(3,4- Ethylenedioxythiophene) Poly-(Styrenesulfonate) (PEDOT/PSS). *Key Eng. Mater.* **2007**, *345-346*, 1189−1192.

(18) Wang, X. S.; Tang, H. P.; Li, X. D.; Hua, X. Investigations on the Mechanical Properties of Conducting Polymer Coating-Substrate Structures and Their Influencing Factors. *Int. J. Mol. Sci.* **2009**, *10*, 5257−5284.

(19) Green, R. A.; Goding, J. A. Biosynthetic Conductive Polymer Composites for Tissue-Engineering Biomedical Devices. In *Biosynthetic Polymers for Medical Applications*; Poole-Warren, L., Martens, P., Green, R. B. T., Eds.; Woodhead Publishing, 2016; pp. 277−298. DOI: 10.1016/B978-1-78242-105-4.00011-0.

(20) Guo, B.; Ma, P. X. Conducting Polymers for Tissue Engineering. *Biomacromolecules* **2018**, *19*, 1764−1782.

(21) Jafarkhani, M.; Salehi, Z.; Nematian, T. Preparation and Characterization of Chitosan/Graphene Oxide Composite Hydrogels for Nerve Tissue Engineering. *Mater. Today: Proc.* **2018**, *5*, 15620−15628.

(22) Yuk, H.; Lu, B.; Zhao, X. Hydrogel Bioelectronics. *Chem. Soc. Rev.* **2019**, *48*, 1642−1667.

(23) Mandal, S.; Seth, A.; Yadav, V.; Kumari, S.; Kumar, M.; Ojha, U. Nanocomposite Grafted Stretchable and Conductive Ionic Hydrogels for Use as Soft Electrode in a Wearable Electrocardiogram Monitoring Device. *ACS Appl. Polym. Mater.* **2020**, *2*, 618−625.

(24) Yang, S.; Jang, L.; Kim, S.; Yang, J.; Yang, K.; Cho, S. W.; Lee, J. Y. Polypyrrole/Alginate Hybrid Hydrogels: Electrically Conductive and Soft Biomaterials for Human Mesenchymal Stem Cell Culture and Potential Neural Tissue Engineering Applications. *Macromol. Biosci.* **2016**, *16*, 1653−1661.

(25) Nam, J.; Lim, H.-K.; Kim, N. H.; Park, J. K.; Kang, E. S.; Kim, Y.-T.; Heo, C.; Lee, O.-S.; Kim, S.-G.; Yun, W. S.; Suh, M.; Kim, Y. H. Supramolecular Peptide Hydrogel-Based Soft Neural Interface Augments Brain Signals through Three-Dimensional Electrical Network. *ACS Nano* **2020**, *14*, 664−675.

(26) Boni, R.; Ali, A.; Shavandi, A.; Clarkson, A. N. Current and Novel Polymeric Biomaterials for Neural Tissue Engineering. *J. Biomed. Sci.* **2018**, *25*, 90.

(27) Green, R.; Abidian, M. R. Conducting Polymers for Neural Prosthetic and Neural Interface Applications. *Adv. Mater.* **2015**, *27*, 7620−7637.

(28) Liu, X.; Miller, A. L., II; Park, S.; Waletzki, B. E.; Terzic, A.; Yaszemski, M. J.; Lu, L. Covalent Crosslinking of Graphene Oxide and Carbon Nanotube into Hydrogels Enhances Nerve Cell Responses. *J. Mater. Chem. B* **2016**, *4*, 6930−6941.

(29) Imaninezhad, M.; Pemberton, K.; Xu, F.; Kalinowski, K.; Bera, R.; Zustiak, S. P. Directed and Enhanced Neurite Outgrowth Following Exogenous Electrical Stimulation on Carbon Nanotube-Hydrogel Composites. *J. Neural Eng.* **2018**, *15*, No. 056034.

(30) Pierini, F.; Guglielmelli, A.; Urbanek, O.; Nakielski, P.; Pezzi, L.; Buda, R.; Lanzi, M.; Kowalewski, T. A.; De Sio, L. Thermoplasmonic-Activated Hydrogel Based Dynamic Light Attenuator. *Adv. Opt. Mater.* **2020**, *8*, 2000324.

(31) Min, J. H.; Patel, M.; Koh, W.-G. Incorporation of Conductive Materials into Hydrogels for Tissue Engineering Applications. *Polymers (Basel).* **2018**, *10*, 1−36.

(32) Huang, B. Carbon Nanotubes and Their Polymeric Composites: The Applications in Tissue Engineering. *Biomanuf. Rev.* **2020**, *5*, 3.

(33) Bei, H.; Yang, Y.; Zhang, Q.; Tian, Y.; Luo, X.; Yang, M.; Zhao, X. Graphene-Based Nanocomposites for Neural Tissue Engineering. *Molecules* **2019**, *24*, 658.

(34) Shi, Y.; Ma, C.; Peng, L.; Yu, G. Conductive "Smart" Hybrid Hydrogels with PNIPAM and Nanostructured Conductive Polymers. *Adv. Funct. Mater.* **2015**, *25*, 1219−1225.

(35) Chakraborty, P.; Bairi, P.; Roy, B.; Nandi, A. K. Improved Mechanical and Electronic Properties of Co-Assembled Folic Acid Gel with Aniline and Polyaniline. *ACS Appl. Mater. Interfaces* **2014**, *6*, 3615−3622.

(36) Ansari, S. P.; Anis, A. Conducting Polymer Hydrogels. In *Polymeric Gels*; Pal, K., Banerjee, I. B. T., Eds.; Woodhead Publishing, 2018; pp. 467−486. DOI: 10.1016/B978-0-08-102179-8.00018-1.

(37) Roland, C. M. Encyclopedia of Polymeric Nanomaterials. In *Encyclopedia of Polymeric Nanomaterials*; Kobayashi, S., Müllen, K., Eds.; Springer Berlin Heidelberg, 2015; pp. 1−9. DOI: 10.1007/978-3-642-36199-9.

(38) Myung, D.; Waters, D.; Wiseman, M.; Duhamel, P.-E.; Noolandi, J.; Ta, C. N.; Frank, C. W. Progress in the Development of Interpenetrating Polymer Network Hydrogels. *Polym. Adv. Technol.* **2008**, *19*, 647−657.

(39) Goding, J.; Gilmour, A.; Martens, P.; Poole-Warren, L.; Green, R. Interpenetrating Conducting Hydrogel Materials for Neural Interfacing Electrodes. *Adv. Healthcare Mater.* **2017**, *6*, 1601177.

(40) Kleber, C.; Bruns, M.; Lienkamp, K.; Rühe, J.; Asplund, M. An Interpenetrating, Microstructurable and Covalently Attached Conducting Polymer Hydrogel for Neural Interfaces. *Acta Biomater.* **2017**, *58*, 365−375.

(41) Distler, T.; Boccaccini, A. R. 3D Printing of Electrically Conductive Hydrogels for Tissue Engineering and Biosensors − A Review. *Acta Biomater.* **2020**, *101*, 1−13.

(42) Yuk, H.; Lu, B.; Lin, S.; Qu, K.; Xu, J.; Luo, J.; Zhao, X. 3D Printing of Conducting Polymers. *Nat. Commun.* **2020**, *11*, 1604.

(43) Wang, F.; Li, M.; Wang, B.; Zhang, J.; Cheng, Y.; Liu, L.; Lv, F.; Wang, S. Synthesis and Characterization of Water-Soluble Polythiophene Derivatives for Cell Imaging. *Sci. Rep.* **2015**, *5*, 7617.

(44) Das, S.; Chatterjee, D. P.; Ghosh, R.; Nandi, A. K. Water Soluble Polythiophenes: Preparation and Applications. *RSC Adv.* **2015**, *5*, 20160−20177.

(45) Lanzi, M.; Salatelli, E.; Giorgini, L.; Marinelli, M.; Pierini, F. Effect of the Incorporation of an Ag Nanoparticle Interlayer on the Photovoltaic Performance of Green Bulk Heterojunction Water-Soluble Polythiophene Solar Cells. *Polymer (Guildf).* **2018**, *149*, 273−285.

(46) Lanzi, M.; Salatelli, E.; Giorgini, L.; Mucci, A.; Pierini, F.; Di-Nicola, F. P. Water-Soluble Polythiophenes as Efficient Charge-Transport Layers for the Improvement of Photovoltaic Performance in Bulk Heterojunction Polymeric Solar Cells. *Eur. Polym. J.* **2017**, *97*, 378−388.

(47) Pawłowska, S.; Rinoldi, C.; Nakielski, P.; Ziai, Y.; Urbanek, O.; Li, X.; Kowalewski, T. A.; Ding, B.; Pierini, F. Ultraviolet Light-Assisted Electrospinning of Core−Shell Fully Cross-Linked P(NIPAAm-Co-NIPMAAm) Hydrogel-Based Nanofibers for Thermally Induced Drug Delivery Self-Regulation. *Adv. Mater. Interfaces* **2020**, *7*, 2000247.

(48) Nakielski, P.; Pawłowska, S.; Rinoldi, C.; Ziai, Y.; De Sio, L.; Urbanek, O.; Zembrzycki, K.; Pruchniewski, M.; Lanzi, M.; Salatelli, E.; Calogero, A.; Kowalewski, T. A.; Yarin, A. L.; Pierini, F. Multifunctional Platform Based on Electrospun Nanofibers and Plasmonic Hydrogel: A Smart Nanostructured Pillow for Near-Infrared Light-Driven Biomedical Applications. *ACS Appl. Mater. Interfaces* **2020**, *12*, 54328−54342.

(49) Haq, M. A.; Su, Y.; Wang, D. Mechanical Properties of PNIPAM Based Hydrogels: A Review. *Mater. Sci. Eng. C* **2017**, *70*, 842−855.

(50) Cao, M.; Wang, Y.; Hu, X.; Gong, H.; Li, R.; Cox, H.; Zhang, J.; Waigh, T. A.; Xu, H.; Lu, J. R. Reversible Thermoresponsive Peptide−PNIPAM Hydrogels for Controlled Drug Delivery. *Biomacromolecules* **2019**, *20*, 3601−3610.

(51) Sanzari, I.; Buratti, E.; Huang, R.; Tusan, C. G.; Dinelli, F.; Evans, N. D.; Prodromakis, T.; Bertoldo, M. Poly(N-Isopropylacrylamide) Based Thin Microgel Films for Use in Cell Culture Applications. *Sci. Rep.* **2020**, *10*, 6126.

(52) Lanzi, M.; Paganin, L. New Regioregular Polythiophenes Functionalized with Sulfur-Containing Substituents for Bulk Heterojunction Solar Cells. *React. Funct. Polym.* **2010**, *70*, 346−360.

(53) Meynaq, M. Y. K.; Shimizu, K.; Aghbolagh, M. S.; Tesfalidet, S.; Lindholm-Sethson, B. Investigation of Metal Ion Interaction with a Lipid Cubic Phase Using Electrochemical Impedance Spectroscopy. *J. Colloid Interface Sci.* **2016**, *482*, 212−220.

(54) Bard, A. J.; Faulkner, L. R. *Electrochemical Methods: Fundamentals and Applications*; 2nd ed.; Wiley: New York, 2002; Vol. 38. DOI: 10.1023/A:1021637209564.

(55) Kaastrup, K.; Sikes, H. D. Using Photo-Initiated Polymerization Reactions to Detect Molecular Recognition. *Chem. Soc. Rev.* **2016**, *45*, 532−545.

(56) Tourillon, G.; Garnier, F. Electrochemical Doping of Polythiophene in Aqueous Medium: Electrical Properties and Stability. *J. Electroanal. Chem. Interfacial Electrochem.* **1984**, *161*, 407−414.

(57) Struys, T.; Moreels, M.; Martens, W.; Donders, R.; Wolfs, E.; Lambrichts, I. Ultrastructural and Immunocytochemical Analysis of Multilineage Differentiated Human Dental Pulp- and Umbilical Cord-Derived Mesenchymal Stem Cells. *Cells Tissues Organs* **2011**, *193*, 366−378.

(58) Donders, R.; Bogie, J. F. J.; Ravanidis, S.; Gervois, P.; Vanheusden, M.; Marée, R.; Schrynemackers, M.; Smeets, H. J. M.; Pinxteren, J.; Gijbels, K.; Walbers, S.; Mays, R. W.; Deans, R.; Van Den Bosch, L.; Stinissen, P.; Lambrichts, I.; Gyselaers, W.; Hellings, N. Human Wharton's Jelly-Derived Stem Cells Display a Distinct Immunomodulatory and Proregenerative Transcriptional Signature Compared to Bone Marrow-Derived Stem Cells. *Stem Cells Dev.* **2018**, *27*, 65−84.

(59) Fiorelli, R.; Cebrian-Silla, A.; Garcia-Verdugo, J.-M.; Raineteau, O. The Adult Spinal Cord Harbors a Population of GFAP-Positive Progenitors with Limited Self-Renewal Potential. *Glia* **2013**, *61*, 2100−2113.

(60) Sulejczak, D.; Andrychowski, J.; Kowalczyk, T.; Nakielski, P.; Frontczak-Baniewicz, M.; Kowalewski, T. Original ArticleElectrospun Nanofiber Mat as a Protector against the Consequences of Brain Injury. *Folia Neuropathol.* **2014**, *1*, 56−69.

(61) Pawłowska, S.; Kowalewski, T. A.; Pierini, F. Fibrous Polymer Nanomaterials for Biomedical Applications and Their Transport by Fluids: An Overview. *Soft Matter* **2018**, *14*, 8421−8444.

(62) Yi, C.; Xu, Z. Synthesis and Characterization of Thermosensitive Composite Microsphere Latex. *J. Appl. Polym. Sci.* **2005**, *96*, 824−828.

(63) Mawad, D.; Artzy-Schnirman, A.; Tonkin, J.; Ramos, J.; Inal, S.; Mahat, M. M.; Darwish, N.; Zwi-Dantsis, L.; Malliaras, G. G.; Gooding,

J. J.; Lauto, A.; Stevens, M. M. Electroconductive Hydrogel Based on Functional Poly(Ethylenedioxy Thiophene). *Chem. Mater.* **2016**, *28*, 6080−6088.

(64) Rinoldi, C.; Fallahi, A.; Yazdi, I.; Campos Paras, J.; Kijeńska-Gawrońska, E.; Trujillo-de Santiago, G.; Tuoheti, A.; Demarchi, D.; Annabi, N.; Khademhosseini, A.; Swieszkowski, W.; Tamayol, A. Mechanical and Biochemical Stimulation of 3D Multi-Layered Scaffolds for Tendon Tissue Engineering. *ACS Biomater. Sci. Eng.* **2019**, *5*, 2953−2964.

(65) Nair, A.; Shen, J.; Lotfi, P.; Ko, C.-Y.; Zhang, C. C.; Tang, L. Biomaterial Implants Mediate Autologous Stem Cell Recruitment in Mice. *Acta Biomater.* **2011**, *7*, 3887−3895.

(66) Qazi, T. H.; Mooney, D. J.; Duda, G. N.; Geissler, S. Biomaterials That Promote Cell-Cell Interactions Enhance the Paracrine Function of MSCs. *Biomaterials* **2017**, *140*, 103−114.

(67) Rinoldi, C.; Costantini, M.; Kijeńska-Gawrońska, E.; Testa, S.; Fornetti, E.; Heljak, M.; Ćwiklińska, M.; Buda, R.; Baldi, J.; Cannata, S.; Guzowski, J.; Gargioli, C.; Khademhosseini, A.; Swieszkowski, W. Tendon Tissue Engineering: Effects of Mechanical and Biochemical Stimulation on Stem Cell Alignment on Cell-Laden Hydrogel Yarns. *Adv. Healthcare Mater.* **2019**, *8*, 1801218.

(68) Yang, L.; Cheng, F.; Liu, T.; Lu, J. R.; Song, K.; Jiang, L.; Wu, S.; Guo, W. Comparison of Mesenchymal Stem Cells Released from Poly(*N*-Isopropylacrylamide) Copolymer Film and by Trypsinization. *Biomed. Mater.* **2012**, *7*, No. 035003.

(69) Li, G.; Kong, Y.; Zhao, Y.; Zhao, Y.; Zhang, L.; Yang, Y. Fabrication and Characterization of Polyacrylamide/Silk Fibroin Hydrogels for Peripheral Nerve Regeneration. *J. Biomater. Sci., Polym. Ed.* **2015**, *26*, 899−916.

(70) Fiorelli, R.; Azim, K.; Fischer, B.; Raineteau, O. Adding a Spatial Dimension to Postnatal Ventricular-Subventricular Zone Neurogenesis. *Development* **2015**, *142*, 2109−2120.

(71) Sun, X.; Tyagi, P.; Agate, S.; McCord, M. G.; Lucia, L. A.; Pal, L. Highly Tunable Bioadhesion and Optics of 3D Printable PNIPAm/Cellulose Nanofibrils Hydrogels. *Carbohydr. Polym.* **2020**, *234*, 115898.

(72) Arslan, H.; Nojoomi, A.; Jeon, J.; Yum, K. 3D Printing of Anisotropic Hydrogels with Bioinspired Motion. *Adv. Sci.* **2019**, *6*, 1800703.

(73) Han, D.; Lu, Z.; Chester, S. A.; Lee, H. Micro 3D Printing of a Temperature-Responsive Hydrogel Using Projection Micro-Stereolithography. *Sci. Rep.* **2018**, *8*, 1963.

(74) Pawar, A. A.; Saada, G.; Cooperstein, I.; Larush, L.; Jackman, J. A.; Tabaei, S. R.; Cho, N.-J.; Magdassi, S. High-Performance 3D Printing of Hydrogels by Water-Dispersible Photoinitiator Nanoparticles. *Sci. Adv.* **2016**, *2*, No. e1501381.